bioRxiv preprint doi: https://doi.org/10.1101/2021.08.11.456023; this version posted August 12, 2021. The copyright holder for this preprint (which was not certified by peer review) is the author/funder. All rights reserved. No reuse allowed without permission.

1 **Kindlin-2 preserves integrity of the articular cartilage to protect against**
2 **osteoarthritis**
3
4 Xiaohao Wu[1#], Yumei Lai[2#], Sheng Chen[1,3#], Chunlei Zhou[4], Chu Tao[1], Xuekun Fu[1], Jun
5 Li[2], Jian Huang[2], Wei Tong[3], Hongtao Tian[3], Zengwu Shao[3], Chuanju Liu[5], Di Chen[6],
6 Xiaochun Bai[7*], Huiling Cao[1*], Guozhi Xiao[1*]
7
8 [1]Department of Biochemistry, School of Medicine, Southern University of Science and
9 Technology, Guangdong Provincial Key Laboratory of Cell Microenvironment and Disease
10 Research, Shenzhen Key Laboratory of Cell Microenvironment, Shenzhen, 518055,
11 China.
12 [2]Department of Orthopedic Surgery, Rush University Medical Center, Chicago, IL 60612,
13 USA.
14 [3]Department of Orthopedics, Union Hospital, Tongji Medical College, Huazhong
15 University of Science and Technology, Wuhan 430022, Hubei, China.
16 [4]Department of Medical Laboratory, Tianjin First Center Hospital, Tianjin Medical
17 University, Tianjin, 300192, China.
18 [5]Department of Orthopedic Surgery, New York University School of Medicine, New York,
19 NY 10003, United States; Department of Cell Biology, New York University School of
20 Medicine, New York, NY 10016, USA.
21 [6]Research Center for Human Tissues and Organs Degeneration, Shenzhen Institutes of
22 Advanced Technology, Chinese Academy of Sciences, Shenzhen, 518055, China.
23 [7]Guangdong Provincial Key Laboratory of Bone and Joint Degeneration Diseases,
24 Department of Cell Biology, School of Basic Medical Sciences, Southern Medical
25 University, Guangzhou 510515, China.
26 #These authors contributed equally to this study.
27 * Address correspondence to: Dr. Guozhi Xiao, Rm 341, Faculty Research Building 1,
28 Southern University of Science and Technology, 1088 Xueyuan Rd, Shenzhen 518055,

bioRxiv preprint doi: https://doi.org/10.1101/2021.08.11.456023; this version posted August 12, 2021. The copyright holder for this preprint (which was not certified by peer review) is the author/funder. All rights reserved. No reuse allowed without permission.

29 China, Phone: 0755-8801-8488; Email: xiaogz@sustech.edu.cn; Huiling Cao, Rm 312,
30 Faculty Research Building 1, Southern University of Science and Technology, 1088
31 Xueyuan Rd, Shenzhen 518055, China, Phone: 0755-8801-8408; Email:
32 caohl@sustech.edu.cn; Xiaochun Bai, Department of Cell Biology, School of Basic
33 Medical Sciences, Southern Medical University, Guangzhou 510515, China. Phone: 020-
34 6164-8724; Email: baixc15@smu.edu.cn.

35

36 **Key words:** Articular chondrocyte; Kindlin-2; Stat3; Runx2; osteoarthritis.

37 **Running title:** Kindlin-2 protects against OA.

bioRxiv preprint doi: https://doi.org/10.1101/2021.08.11.456023; this version posted August 12, 2021. The copyright holder for this preprint (which was not certified by peer review) is the author/funder. All rights reserved. No reuse allowed without permission.

38 **Abstract**

39 Osteoarthritis (OA) is an aging-related degenerative joint disease, which has no cure
40 partly due to limited understanding of its pathological mechanism(s). Here we report that
41 the focal adhesion protein Kindlin-2, but not Kindlin-1 or -3, is highly expressed in articular
42 chondrocytes of the hyaline cartilage, which is dramatically decreased in the degenerated
43 articular cartilage of aged mice and patients with OA. Inducible deletion of Kindlin-2 in
44 chondrocytes at adult stage leads to spontaneous OA and much severe OA lesions in the
45 mice receiving the surgery of destabilization of the medial meniscus. Mechanistically,
46 Kindlin-2 deficiency promotes mitochondrial oxidative stress and activates Stat3 in
47 articular chondrocytes, leading to Runx2-mediated chondrocyte hypertrophic
48 differentiation and catabolism. In vivo, systemic pharmacological blockade of Stat3
49 activation or genetic ablation of Stat3 in chondrocytes reverses aberrant accumulation of
50 Runx2 and ECM-degrading enzymes and limits OA deteriorations caused by Kindlin-2
51 deficiency. Furthermore, genetic inactivation of Runx2 in chondrocytes reverses
52 structural changes and OA lesions caused by Kindlin-2 deletion without down-regulating
53 p-Stat3 in articular chondrocytes. Of translational significance, intraarticular injection of
54 Kindlin-2-expressing adeno-associated virus decelerates progression of aging- and
55 instability-induced knee joint OA in mice. Collectively, we identify a novel pathway
56 comprising of Kindlin-2, Stat3 and Runx2 in articular chondrocytes responsible for
57 maintaining integrity of the articular cartilage and define a potential therapeutic target for
58 OA.

bioRxiv preprint doi: https://doi.org/10.1101/2021.08.11.456023; this version posted August 12, 2021. The copyright holder for this preprint (which was not certified by peer review) is the author/funder. All rights reserved. No reuse allowed without permission.

59 **Introduction**

60 Osteoarthritis (OA) is the most prevalent degenerative joint disease and the leading cause
61 of chronic disability among elderly people worldwide. The etiologic factors of human OA
62 include aging, joint overuse or injury, obesity and heredity. While OA is a whole joint
63 disease affecting articular cartilage, subchondral bone and synovium, a progressive loss
64 of articular cartilage is a hallmark event of OA pathology (*1*). Molecular mechanisms
65 underlying OA initiation, development and progression remain elusive. As a consequence,
66 there are currently no FDA-approved OA treatments or effective interventions to limit OA
67 progression (*2*). Therefore, it is important to define mechanisms that control the articular
68 cartilage homeostasis under physiological condition and how they are altered under OA
69 state.

70 Chondrocytes are the only cell type in the articular cartilage and are surrounded by
71 a collagen-rich extracellular matrix (ECM), the major target of osteoarthritic cartilage
72 degradation. A hypertrophic and catabolic phenotype characterized by aberrant
73 production of ECM-degrading proteases Mmp13 and Adamts4/5 by articular
74 chondrocytes facilitates ECM degradation and OA initiation and progression (*3, 4*). While
75 integrins are the transmembrane receptors for ECM, whether and how alterations in the
76 ECM-integrin signaling pathway are involved in OA initiation and progression are still
77 controversial (*5-7*). Several studies using genetically modified mouse models reveal that
78 aberrant accumulation of Runx2 protein accelerates articular chondrocyte hypertrophy
79 and stimulates expression of ECM-degrading proteases, leading to OA (*4, 8-14*).
80 Furthermore, activation of the signal transducer and activator of transcription (Stat3)
81 stimulates, while inactivation of Stat3 inhibits, OA initiation and progression (*15-17*).
82 However, key signaling molecules that maintain the articular chondrocyte anabolism and
83 integrity of the articular cartilage remain poorly understood. Furthermore, it is important
84 to investigate whether alterations in expression of these molecules in articular
85 chondrocytes play major roles in pathogenesis of OA.

86 Kindlins are key focal adhesion proteins that interact with the cytoplasmic domain of

bioRxiv preprint doi: https://doi.org/10.1101/2021.08.11.456023; this version posted August 12, 2021. The copyright holder for this preprint (which was not certified by peer review) is the author/funder. All rights reserved. No reuse allowed without permission.

87 the β integrins and activate integrins to regulate cell-ECM adhesion, migration and
88 signaling (*18-20*). In mammalian cells, there are three Kindlin proteins, i.e., Kindlin-1, -2
89 and -3, encoded by *Fermt1*, *Fermt2* and *Fermt3,* respectively (*21, 22*). Human genetic
90 diseases are linked to mutations in Kindlin-1 and -3, but not Kindlin-2 (*23-26*). Kindlin-2
91 is essential for early embryonic development; thus, global inactivation of the gene
92 encoding Kindlin-2 resulted in very early embryonic lethality at E7.5 in mice (*27*). Previous
93 studies of Kindlin-2 primarily focus on its roles in regulation of tumor formation,
94 progression and metastasis (*28*). Recently, increasing attention has been paid to its roles
95 in control of organogenesis and homeostasis through both integrin-dependent and
96 integrin-independent mechanisms (*28-40*). We recently demonstrate that Kindlin-2 plays
97 critical roles in regulation of skeletal development and bone remodeling through distinct
98 molecular mechanisms (*41-44*). However, it is not known whether Kindlin-2 has a role in
99 articular cartilage homeostasis and whether alterations in its expression in articular
100 chondrocytes are involved in OA initiation and progression.

101 In this study, we demonstrate that Kindlin-2, but not Kindlin-1 and -3, is highly
102 expressed in articular chondrocytes of healthy articular cartilage and dramatically down-
103 regulated in the degenerated articular cartilage of aged mice and patients with OA. We
104 demonstrate that Kindlin-2 loss in chondrocytes causes spontaneous OA and
105 exacerbates instability-induced OA in adult mice. Kindlin-2 deficiency promotes
106 hypertrophic differentiation and matrix catabolism through Stat3-dependent up-regulation
107 of Runx2 in articular chondrocytes, leading to OA. Intraarticular injection of AAV5
108 expressing Kindlin-2 attenuates OA damages caused by aging and instability in mice.

bioRxiv preprint doi: https://doi.org/10.1101/2021.08.11.456023; this version posted August 12, 2021. The copyright holder for this preprint (which was not certified by peer review) is the author/funder. All rights reserved. No reuse allowed without permission.

109 **Results**

110 **Kindlin-2, but not Kindlin-1 or -3, is highly expressed in chondrocytes of the hyaline**
111 **articular cartilage in mice and humans.**

112 As an initial step to investigate potential role of the Kindlin proteins in the articular cartilage,
113 we examined their expression by performing the Safranin O & Fast Green (SO&FG) and
114 immunofluorescence (IF) staining of serial knee joint sections from adult C57BL/6 mice
115 using antibodies against Kindlin-1, -2 or -3 (Figure 1a, top). Results revealed that Kindlin-
116 2 was strongly detected in articular chondrocytes of the hyaline cartilage (Figure 1a,b). In
117 contrast, both Kindlin-1 and -3 proteins were not expressed in the articular chondrocytes.
118 It is interesting to observe that expression of Kindlin-2 was essentially lost in chondrocytes
119 of the calcified cartilage (Figure 1a). Similarly, Kindlin-2, but not Kindlin-1 and 3, was
120 highly expressed in articular chondrocytes of the human knee joint cartilage (Figure 1a,c).
121

122 **Kindlin-2 expression is drastically reduced in the degenerated articular cartilage of**
123 **aged mice and patients with OA.**

124 We found that the number of Kindlin-2-positive articular chondrocytes in the knee joints
125 was decreased by 4-fold in aged (24 mo) mice compared to that in young (2 mo) mice
126 (Figure 1d-f) (64% in 2 mo versus 16% in 24 mo, $P < 0.0005$, Student's *t* test). It should
127 be noted that 24-mo-old mice displayed a dramatic degeneration of the knee joint articular
128 cartilage (Figure 1d). We next obtained human knee joint cartilage samples from total
129 knee arthroplasty (TKA) (Figure 1g). As expected, OA cartilage displayed a dramatic
130 increase in OARSI (Osteoarthritis Research Society International) score (Figure 1h) and
131 a decrease in aggrecan-containing cartilage (Figure 1i). Please note a vertical fissure in
132 OA cartilage (Figure 1i). Results from IF staining showed a drastic reduction in expression
133 of aggrecan in OA versus normal cartilage (Figure 1j). The percentages of Kindlin-2-, talin-
134 and vinculin-positive cells were all dramatically reduced in OA relative to normal cartilage
135 (Figure 1j-m), while those of both Col10a1- and Mmp13-positive cells were significantly
136 increased in OA versus normal cartilage (Figure 1j,n,o). The percentage of Kindlin-2-

bioRxiv preprint doi: https://doi.org/10.1101/2021.08.11.456023; this version posted August 12, 2021. The copyright holder for this preprint (which was not certified by peer review) is the author/funder. All rights reserved. No reuse allowed without permission.

137 positive articular chondrocytes was decreased by 2.7-fold in OA versus normal cartilage
138 (Figure 1k) (56.25% in Normal versus 21.2% in OA, $P < 0.0001$, Student's *t* test). Note:
139 the expression level of p-FAK was extremely low in both OA and normal cartilage (Figure
140 1j).
141

142 **Inducible deletion of Kindlin-2 in chondrocytes at adult stage causes striking**
143 **spontaneous OA-like phenotype.**

144 Based on above observations, we wondered whether the loss of Kindlin-2 in articular
145 chondrocytes plays a role in promotion of OA development and progression. To test if this
146 is the case, we generated mice bearing conditional alleles of *Kindlin-2* and
147 *Aggrecan*^{CreERT2}, i.e., *K2*$^{fl/fl}$*; Aggrecan*^{CreERT2} (Supplementary Figure 1). Note: a high Cre-
148 recombination efficiency was observed in the knee joint articular chondrocytes, but not in
149 cells of the synovium, in *Aggrecan*^{CreERT2} mice at 4 weeks after tamoxifen injections
150 (Supplementary Figure 2a). At 2 months of age, *K2*$^{fl/fl}$*; Aggrecan*^{CreERT2} mice were
151 subjected to five daily injections of tamoxifen (TM) (100 mg/kg body weight) to generate
152 the chondrocyte conditional Kindlin-2 knockout mice (hereafter referred to as cKO)
153 (Figure 2a). The *K2*$^{fl/fl}$*; Aggrecan*^{CreERT2} mice injected with corn oil were used as controls
154 in this study. At 6 months after TM injection (same hereinafter), we observed a marked
155 enlargement of the knee joint (left panel, red dashed line) (Figure 2b), an excessive tibial
156 plateau angle (middle panel, red double headed arrow) (Figure 2b) and articular cartilage
157 damage of the femoral condyles (right panel, red arrows) in cKO mice (Figure 2b). X-ray
158 micro-computerized tomography (μCT) imaging of the knee joints revealed increasing
159 osteophyte formation in cKO but not in control mice (Figure 2c,d and Supplementary
160 Figure 3a). cKO mice displayed increased volume of calcified meniscus and synovium
161 (Figure 2d) and hyperalgesia (Figure 2e). Kindlin-2 loss caused a dramatic loss of the
162 articular cartilage, as demonstrated by a dramatic increase in OARSI score and a
163 decrease in cartilage area in cKO mice (Figure 2f,i,j and Supplementary Figure 3b-d).
164 Kindlin-2 loss stimulated a synovial hyperplasia (Figure 2g,l). At the molecular level, the

bioRxiv preprint doi: https://doi.org/10.1101/2021.08.11.456023; this version posted August 12, 2021. The copyright holder for this preprint (which was not certified by peer review) is the author/funder. All rights reserved. No reuse allowed without permission.

165 numbers of Runx2-, Col10a1- and Mmp13-positive cells were dramatically increased in
166 cKO versus control articular cartilage (Figure 2h,m-p and Supplementary Figure 4a-f). In
167 fact, those cells were rarely observed in control articular cartilage. As expected, Runx2-
168 positive cells were also detected in the calcified cartilage, subchondral bone and bone
169 marrow in both control and cKO mice.

170 Collectively, we demonstrate that Kindlin-2 loss in adult mice promotes expression
171 of Runx2, chondrocyte hypertrophic and catabolic phenotype, and spontaneous OA-like
172 phenotypes, including progressive cartilage loss and structural deterioration, osteophyte
173 outgrowth, synovial hyperplasia and pain, which mimic major pathological features of
174 human OA.

175

176 **Kindlin-2 deficiency in chondrocytes at adult stage exacerbates instability-induced**
177 **OA.**

178 We further investigated whether Kindlin-2 loss impacts progression of the injury-induced
179 OA by utilizing a well-established destabilization of the medial meniscus (DMM) mouse
180 OA model. At 2 months of age, the *K2*$^{fl/fl}$*; Aggrecan*^{CreERT2} mice were subjected to sham
181 or DMM surgery. One week later, mice were injected with TM (cKO) or corn oil (control)
182 as indicated in Figure 3a. At 8 weeks after surgery, we performed μCT scans and
183 histomorphometrical analyses of SO&FG and H/E-stained knee joint sections to evaluate
184 knee joint damages (Figure 3b-e). At this time point, cKO mice did not display marked
185 abnormalities in the volume of calcified meniscus and synovial tissue (Figure 3c), OARSI
186 score (Figure 3f), cartilage area (Figure 3g), osteophyte score (Figure 3h) and synovitis
187 score (Figure 3i). As expected, when compared to control mice with sham operation,
188 control mice with DMM (control-DMM) exhibited apparent OA lesions, as revealed by a
189 dramatic loss of the articular cartilage, synovial hyperplasia and osteophyte outgrowth
190 (Figure 3b-i) (P < 0.05, control-sham vs control-DMM for all indicated parameters).
191 Importantly, cKO mice with DMM (cKO-DMM) displayed more severe OA phenotypes
192 than control-DMM did (Figure 3b-i) (P < 0.05, control-DMM vs cKO-DMM for all indicated

bioRxiv preprint doi: https://doi.org/10.1101/2021.08.11.456023; this version posted August 12, 2021. The copyright holder for this preprint (which was not certified by peer review) is the author/funder. All rights reserved. No reuse allowed without permission.

193 parameters). Collectively, Kindlin-2 deletion in chondrocytes exacerbates OA lesions
194 caused by instability in mice.
195

196 **Kindlin-2 loss up-regulates expression of p-Sta3, Runx2, Col10a1 and ECM-**
197 **degrading proteases in articular chondrocytes.**

198 We performed RNA sequencing analysis using total RNA from the knee joints of control
199 and cKO mice at 5 months after TM injections. Results from KEGG pathway analysis
200 revealed significant enrichment of several signaling pathways, including the JAK-STAT3
201 and NF-κB signaling pathways (Figure 4a). Consistent with results from the RNAseq
202 analysis, knockdown of Kindlin-2 increased the protein levels of p-Stat3 (but not its total
203 protein, t-Stat3) in ATDC5 cells and in primary articular chondrocytes (Figure 4b,c and
204 Supplementary Figures 5, 6). Furthermore, Kindlin-2 loss increased the protein levels of
205 Runx2, Col10a1, Mmp13 and Adamts5 in ATDC5 cells and in primary articular
206 chondrocytes (Figure 4b,c and Supplementary Figures 5, 6). IF staining showed that
207 Kindlin-2 knockdown increased expression of p-Stat3 in nuclei of ATDC5 cells and that
208 of p-Stat3 and Runx2 in primary articular chondrocytes (Figure 4d and Supplementary
209 Figure 6e). Furthermore, Kindlin-2 knockdown increased the protein level of p-Stat3
210 (Y705), but not p-Stat3 (Y727), in ATDC5 cells (Figure 4e and Supplementary Figure 7a).
211 Results from IF staining of serial sections of the knee joints revealed that percentage of
212 p-Stat3-positive chondrocytes was drastically increased in cKO versus control cartilage
213 (Figure 4f,g). Furthermore, the percentage of activated β1 integrin-positive cells was
214 significantly reduced, whereas the percentages of p-p38-, p-Erk- and p-Jak2-positive cells
215 were not significantly altered in cKO articular cartilages compared to those in control
216 articular cartilages (Supplementary Figure 8a-e). Loss of Kindlin-2 markedly impaired the
217 attachment and spreading of primary articular chondrocytes on collagen-II coated surface
218 in vitro (Supplementary Figure 9).
219

220 **Loss of Kindlin-2 expression associates with elevations of p-Stat3 and Runx2 in**

bioRxiv preprint doi: https://doi.org/10.1101/2021.08.11.456023; this version posted August 12, 2021. The copyright holder for this preprint (which was not certified by peer review) is the author/funder. All rights reserved. No reuse allowed without permission.

221 **articular chondrocytes during aging and OA development.**
222 Western blotting using protein extracts from articular cartilage of mice with different ages
223 showed that expression of Kindlin-2 was reduced and that of p-Stat3 and Runx2 was
224 increased in aged (18 mo) versus young (2 mo) mice (Figure 4h,i). SO&FG and IF staining
225 of serial knee joints sections of mice with different ages showed that the percentages of
226 Kindlin-2-positive chondrocytes were decreased and those of p-Stat3- and Runx2-
227 positive chondrocytes were increased in aged versus young cartilages (Figure 4j,k).
228 Quantitative data showed that the severity of aging-induced OA, as measured by
229 increases in OARSI score and osteophyte score and decrease in cartilage area, was
230 closely correlated to the magnitude of Kindlin-2 down-regulation or p-Stat3 and Runx2
231 up-regulation in articular chondrocytes (Figure 4l-q). In humans, the percentages of p-
232 Stat3- and Runx2-positive chondrocytes were increased by 2.7- and 4.5-fold, respectively,
233 in OA relative to normal cartilage ($P < 0.0001$, normal versus OA, Student's *t* test) (Figure
234 4r,t,u). Again, the percentage of Kindlin-2-positive chondrocytes was decreased in human
235 OA versus normal cartilage (Figure 4r,s).
236
237 **Kindlin-2 deficiency stimulates chondrocyte hypertrophic differentiation and**
238 **catabolism through Stat3-dependent up-regulation of Runx2 expression.**
239 Runx2 is known to activate expression of Col10a1 and Mmp13, which plays a pivotal role
240 in ECM calcification and OA initiation and progression (*3, 4, 8, 9*). Interestingly, siRNA
241 knockdown of Runx2 essentially abolished Kindlin-2 loss-stimulated up-regulation of
242 Col10a1, Mmp13 and Adamts5 without down-regulating expression of p-Stat3 (Figure 4v
243 and Supplementary Figure 7b,d). A previous in vitro study showed that Stat3
244 transcriptionally activates expression of Runx2 to promote human osteoblastic
245 differentiation (*45*). Based on these observations, we wondered whether Kindlin-2 loss
246 stimulates the chondrocyte hypertrophic and catabolic phenotypes by up-regulating
247 Runx2 through Stat3. In support of this notion, we found that siRNA knockdown of Stat3
248 largely reversed the Runx2 mRNA and protein accumulation caused by Kindlin-2 loss

bioRxiv preprint doi: https://doi.org/10.1101/2021.08.11.456023; this version posted August 12, 2021. The copyright holder for this preprint (which was not certified by peer review) is the author/funder. All rights reserved. No reuse allowed without permission.

249 (Figure 4w and Supplementary Figures 7c,e,f). Furthermore, Stat3 knockdown essentially
250 abolished the up-regulation of Col10a1, Mmp13 and Adamts5 caused by Kindlin-2 loss
251 (Figure 4w and Supplementary Figure 7c,e,f). Stat3 siRNA decreased, while Stat3
252 overexpression increased, the level of Runx2 protein in ATDC5 cells (Supplementary
253 Figure 7g,h). Collectively, these results suggest that Kindlin-2 deficiency induces
254 chondrocyte hypertrophic differentiation and catabolism by Stat3-dependent up-
255 regulation of Runx2 in chondrocytes.
256

257 **Kindlin-2 loss accumulates reactive oxygen species (ROS) to activate Stat3 in**
258 **chondrocytes.**

259 We recently reported that a fraction of the Kindlin-2 was present in mitochondrion of lung
260 cancer cells (*34*). Consistent with this finding, Kindlin-2 was also detected in extracts of
261 the mitochondrial fraction of primary articular chondrocytes (Figure 5a). This result was
262 specific because the voltage-dependent anion channel (Vadc), a mitochondrial marker,
263 was detected in mitochondrial but not cytoplasmic fraction of chondrocytes (Figure 5a).
264 Since mitochondrion is the primary source for the intracellular reactive oxygen species
265 (ROS) (*46*), we determined whether Kindlin-2 loss increases ROS production in
266 chondrocytes. Strikingly, we found that the level of mitochondrial ROS, as visualized by
267 the MitoSOX red staining of the knee joint sections, was dramatically elevated in articular
268 chondrocytes or cartilage extracts from the knee joint of cKO mice at 3 months after TM
269 injections (Figure 5b,e). Furthermore, siRNA knockdown of Kindlin-2 increased the level
270 of mitochondrial ROS in ATDC5 cells (Figure 5c,d). Interestingly, excessive oxidative
271 stress in articular chondrocytes was observed in the damaged knee joint articular
272 cartilage from human OA patients, as revealed as OxyIHC staining (Figure 5f,g). H_2O_2, a
273 common ROS in the cells, dose-dependently increased the levels of p-Stat3 and Runx2
274 proteins without affecting expression of t-Stat3 protein in primary articular chondrocytes
275 (Figure 5h). Furthermore, up-regulations of p-Stat3, Runx2, Col10a1 and Mmp13 caused
276 by Kindlin-2 knockdown were largely reversed by N-acetyl cysteine (NAC) (Figure 5i), a

bioRxiv preprint doi: https://doi.org/10.1101/2021.08.11.456023; this version posted August 12, 2021. The copyright holder for this preprint (which was not certified by peer review) is the author/funder. All rights reserved. No reuse allowed without permission.

277 potent ROS scavenger.

278

279 **Kindlin-2 interacts with Stat3 and inhibits Stat3 nuclear translocation in**
280 **chondrocytes.**

281 To further explore mechanisms through which Kindlin-2 deficiency activates Stat3, we
282 determined whether Kindlin-2 interacts with Stat3 by performing immunofluorescence (IF)
283 staining and observed a strong colocalization of both factors in the cytoplasm of primary
284 articular chondrocytes (Figure 5j). We further conducted co-immunoprecipitation (co-IP)
285 assays using whole cell extracts isolated from the COS-7 cells overexpressing Flag-Stat3
286 and Kindlin-2 and found that Stat3 was present in the Kindlin-2 immunoprecipitates
287 (Figure 5k) and, vice versa, that Kindlin-2 was present in the Stat3 immunoprecipitates
288 (Figure 5l). Endogenous Kindlin-2 and Stat3 interacted in primary articular chondrocytes
289 (Figure 5m). H_2O_2-induced increase in p-Stat3 was abolished by overexpression of
290 Kindlin-2 in ATDC5 cells (Figure 5n,o). Overexpression of Kindlin-2 decreased Stat3
291 nuclear translocation in ATDC5 cells stimulated by H_2O_2 (Figure 5p). Finally, H_2O_2 dose-
292 dependently inhibited the Kindlin-2-Stat3 interaction in primary articular chondrocytes
293 (Figure 5q).

294

295 **Systemic pharmacological blockade of Stat3 activation palliates cartilage**
296 **degeneration and osteophyte formation caused by Kindlin-2 loss in mice.**

297 We next determined whether Stat3 activation plays a role in Kindlin-2 loss induction of
298 OA by investigating whether systemic inhibition of Stat3 activation by Stattic can mitigate
299 the OA lesions caused by Kindlin-2 loss in mice. In this experiment, at 8 weeks of age,
300 *$K2^{fl/fl}$; $Aggrecan^{CreERT2}$* mice were performed with DMM surgeries. One week later, mice
301 were subjected to TM injections and administration of Stattic through gavage as
302 implicated in Supplementary Figure 10a. Eight weeks later, mice with DMM displayed
303 marked restriction of movement of the hind limb, which was improved by Stattic
304 (Supplementary Figure 10b). Expression of p-Stat3 was strongly detected in cKO mice

bioRxiv preprint doi: https://doi.org/10.1101/2021.08.11.456023; this version posted August 12, 2021. The copyright holder for this preprint (which was not certified by peer review) is the author/funder. All rights reserved. No reuse allowed without permission.

305 treated with PBS, which was essentially abolished by Stattic (Supplementary Figure 10c).
306 Furthermore, cartilage loss and osteophyte formation caused by Kindlin-2 deletion were
307 attenuated by Stattic treatment (Supplementary Figure 10c-f). However, synovial
308 hyperplasia in cKO mice was not improved by Stattic (Supplementary Figure 10c,g).
309

310 **Genetic deletion of Stat3 in chondrocytes reverses aberrant Runx2 accumulation**
311 **and ameliorates OA lesions caused by Kindlin-2 deficiency in mice.**

312 To obtain further in vivo evidence that Kindlin-2 deletion causes OA by activation of Stat3,
313 we deleted Stat3 expression in chondrocytes and determined its effects on Runx2
314 expression and OA lesions caused by Kindlin-2 deletion in mice with and without DMM.
315 We crossed the $K2^{fl/fl}$; $Aggrecan^{CreERT2}$ (cKO) mice with floxed Stat3 mice ($Stat3^{fl/fl}$) and
316 generated $K2^{fl/fl}$; $Stat3^{fl/fl}$; $Aggrecan^{CreERT2}$ mice (hereinafter referred to as ^{KS}dKO). At 8
317 weeks of age, cKO and ^{KS}dKO mice were subjected to five TM injections as indicated in
318 Figure 6a (top). Mice were killed at 18 weeks of age. Separately, 8-week-old cKO and
319 ^{KS}dKO mice were subjected to DMM surgery, followed by TM treatment as indicated in
320 Figure 6a (bottom). Mice were sacrificed at 16 weeks of age. Results revealed that
321 deletion of Stat3 in chondrocyte corrected the increased OARSI score, osteophyte score
322 and pain and decreased articular cartilage area caused by Kindlin-2 deletion in mice with
323 and without DMM (Figure 6b,c,e-g,i m-o,q). Consistent with results from above Stattic
324 inhibition experiment, Stat3 deletion did not reverse the synovitis stimulated by Kindlin-2
325 deletion in mice with and without DMM (Figure 6c,h,p). At the molecular level, Stat3
326 deletion essentially abolished expression of both Runx2 and Col10a1 in articular
327 chondrocytes (Figure 6d,j-l,r-t). As expected, the number of Stat3-positive cells was
328 dramatically decreased in articular chondrocytes in ^{KS}dKO mice with and without DMM
329 (Figure 6j,r). Note: deleting one allele of *Stat3* gene in chondrocytes slightly but
330 significantly reversed the cartilage loss caused by Kindlin-2 deletion in cKO mice
331 (Supplementary Figure 12a-c). Collectively, these results support our hypothesis that
332 Stat3 activation plays a critical role in mediation of Kindlin-2 loss-induced Runx2 up-

bioRxiv preprint doi: https://doi.org/10.1101/2021.08.11.456023; this version posted August 12, 2021. The copyright holder for this preprint (which was not certified by peer review) is the author/funder. All rights reserved. No reuse allowed without permission.

333 regulation in chondrocytes and OA lesions.
334

335 **Deleting Runx2 in chondrocytes reverses OA defects without reducing p-Stat3**
336 **expression caused by Kindlin-2 deletion in mice.**

337 The next question we asked was whether Runx2 is a major downstream effector of Stat3
338 in mediation of Kindlin-2 loss-caused OA lesions. We determined whether genetic
339 ablation of Runx2 in chondrocytes can limit the OA lesions caused by Kindlin-2 deletion
340 in mice. We bred the $K2^{fl/fl}$; $Aggrecan^{CreERT2}$ (cKO) with floxed Runx2 mice ($Runx2^{fl/fl}$) and
341 generated $K2^{fl/fl}$; $Runx2^{fl/fl}$; $Aggrecan^{CreERT2}$ mice (hereinafter referred to as ^{KR}dKO). We
342 performed two separate sets of experiments on these mice. In the first set of experiment,
343 at 8 weeks of age, cKO and ^{KR}dKO mice were treated with TM as indicated in Figure 7a.
344 At 6 and 12 weeks after TM injection, mice were killed, followed by IF staining and
345 histological and μCT analyses of the knee joints. At 12 weeks, we observed significant
346 osteophyte outgrowth in cKO mice, which was essentially abolished in ^{KR}dKO mice
347 (Figure 7b,e). A dramatic cartilage loss was observed in cKO mice at 12 weeks, but not
348 at 6-weeks (Figure 7c). The cartilage degeneration and pain caused by Kindlin-2
349 deficiency were largely attenuated by Runx2 deletion (Figure 7c,f,g). It is important to
350 note that expression of p-Stat3 in chondrocytes was not reduced in ^{KR}dKO mice (Figure
351 7d). As expected, expression of both Kindlin-2 and Runx2 was essentially abolished in
352 ^{KR}dKO articular chondrocytes (Figure 7d).

353 In the second set of experiment, cKO and ^{KR}dKO mice were subjected to DMM
354 surgery and TM injections as indicated in Figure 7a. At 8 weeks after DMM surgery, cKO
355 mice displayed marked OA lesions with dramatic cartilage loss, osteophyte formation and
356 pain. These OA lesions were largely reversed in ^{KR}dKO mice (Figure 7h-l). Furthermore,
357 the structural deterioration of the knee joint caused by Kindlin-2 deficiency was largely
358 ameliorated in ^{KR}dKO mice (Figure 7h,i). It should be noted that the cartilage loss caused
359 by Kindlin-2 deletion in cKO mice was partially reversed by Runx2 haploinsufficiency in
360 chondrocytes (Supplementary Figure 13a-c).

bioRxiv preprint doi: https://doi.org/10.1101/2021.08.11.456023; this version posted August 12, 2021. The copyright holder for this preprint (which was not certified by peer review) is the author/funder. All rights reserved. No reuse allowed without permission.

361 **Intraarticular injection of Kindlin-2-expressing adeno-associated virus decelerates**
362 **progression of DMM- and aging-induced OA in mice.**
363 We next determined whether overexpression of Kindlin-2 via intraarticular injection of
364 Kindlin-2-expressing adeno-associated virus 5 (AAV5) protects against OA development
365 and progression caused by DMM or aging in mice as indicated in Figure 8a. Efficiency of
366 AAV infection in articular chondrocytes was assessed by intraarticular injection of AAV5
367 expressing enhanced green fluorescent protein (EGFP). Three weeks after injection,
368 strong GFP signal was detected in articular chondrocytes (Figure 8b). Kindlin-2
369 expressing AAV (AAV5-K2) (5×10^9 particles in 10 μl) or control AAV (AAV5-Con) was
370 intraarticularly injected as we previously described (*11*). Results showed that intraarticular
371 injection of AAV5-K2 markedly increased expression of Kindlin-2 in articular chondrocytes
372 of mice with and without DMM (Figure 8c,e). Importantly, DMM caused dramatic cartilage
373 loss, osteophyte formation, synovial hyperplasia and pain, which were largely ameliorated
374 by AAV5-K2 injection as compared with AVV5-Con group (Figure 8d, f-j). More
375 importantly, aging-induced OA lesions were markedly protected by intraarticular injection
376 of AAV5-K2 (Figure 8k-o). Taken together, these results suggest that targeted expression
377 of Kindlin-2 in articular chondrocytes preserves integrity of articular cartilage and protect
378 against aging- and instability-induced OA.
379

380 ## Discussion
381 In this study, we present the first demonstration that the focal adhesion protein Kindlin-2
382 maintains the articular chondrocyte anabolism to preserve integrity of the articular
383 cartilage. We demonstrate that Kindlin-2 acts as a critical intrinsic inhibitor of Runx2
384 expression through inactivation of Stat3 in articular chondrocytes. We show that Kindlin-
385 2 deletion in chondrocytes causes striking and spontaneous OA-like phenotypes,
386 including a progressive loss of the articular cartilage, osteophyte outgrowth, synovial
387 hyperplasia and pain, which highly mimic major features of the aging-associated OA in
388 humans. We show that Kindlin-2 loss accelerates progression of instability-induced OA in

bioRxiv preprint doi: https://doi.org/10.1101/2021.08.11.456023; this version posted August 12, 2021. The copyright holder for this preprint (which was not certified by peer review) is the author/funder. All rights reserved. No reuse allowed without permission.

389 adult mice. In both mouse and OA articular cartilage, chondrocytes display reduced
390 expression of Kindlin-2 and increased expression of p-Stat3 and Runx2 proteins. Of
391 translational significance, intraarticular injection of Kindlin-2-expressing AAV5
392 ameliorates aging-related and DMM-induced OA lesions in mice. Importantly, we provide
393 strong evidence that Kindlin-2 deficiency causes OA by up-regulating Runx2 through
394 promotion of activation and nuclear translocation of Stat3 in articular chondrocytes. These
395 findings highlight a requirement to determine whether abnormalities in expression and/or
396 activity of Kindlin-2, Stat3 and Runx2 in articular chondrocytes play important roles in
397 human OA initiation, development and progression. We may define a useful therapeutic
398 target for OA.

399 Several studies reported that activation of Stat3 is involved in promotion of OA
400 initiation and progression (*15-17*). However, physiological signals that inhibits Stat3
401 activation in articular chondrocytes are unclear. In the present study, we identify Kindlin-
402 2 as an intrinsic and potent inhibitor of the Stat3 activation in articular chondrocytes and
403 plays an important role in maintaining the anabolic status of articular cartilage. The loss
404 of Kindlin-2 largely activates Stat3 by increasing its phosphorylation at Y705, while
405 overexpression of Kindlin-2 exerts an opposite effect. siRNA knockdown of Stat3 in
406 chondrocytes reverses the catabolic gene expression pattern caused by Kindlin-2 loss.
407 Interestingly, we find that expression of p-Jak2, a canonical activator of Stat3, is not
408 markedly altered in Kindlin-2 deficient chondrocytes, suggesting that Kindlin-2 loss
409 induced Stat3 activation is not through Jak2 activation. Most importantly, systemic
410 inhibition of Stat3 activation by Stattic or genetic deletion of Stat3 in chondrocytes in mice
411 largely corrects OA lesions, such as cartilage degeneration and osteophyte formation,
412 caused by Kindlin-2 deficiency. These findings, along with our observation that Stat3 is
413 greatly activated in the damaged OA articular cartilage in patients, suggest that Stat3
414 activation may play an important role in the pathogenesis of human OA. This requires
415 further investigation.

416 Cumulative evidence points to aberrant accumulation of Runx2 protein in articular

bioRxiv preprint doi: https://doi.org/10.1101/2021.08.11.456023; this version posted August 12, 2021. The copyright holder for this preprint (which was not certified by peer review) is the author/funder. All rights reserved. No reuse allowed without permission.

417 chondrocytes being a major player in promoting OA initiation and progression. The loss
418 of Runx2 in chondrocytes provides a significant protection against initiation and
419 progression of instability-induced OA in genetic mouse models, while gain of function of
420 Runx2 stimulates OA development in multiple genetic mouse models (*4, 10-14, 47, 48*).
421 Therefore, it is critical to keep expression of Runx2 in articular chondrocytes under control
422 to preserve integrity of the articular cartilage. Importantly, in the present study, we identify
423 Kindlin-2 as a major player in this respect. We provide multiple lines of molecular and
424 genetic evidence supporting that Kindlin-2 inhibits expression of Runx2 by suppressing
425 Stat3 actions in articular chondrocytes, First, p-Stat3 and Runx2 are in parallel up-
426 regulated in chondrocytes by Kindlin-2 loss in vitro and in cartilage as well as in the aged
427 or damaged articular cartilage of mice and humans with OA. Second, loss of function of
428 Stat3 decreases expression of Runx2 and reverses the chondrocyte catabolic phenotype
429 caused by Kindlin-2 loss in vitro. Third and most importantly, genetic deletion of Stat3 in
430 chondrocytes abolishes Runx2 accumulation and limits OA lesions caused by Kindlin-2
431 loss in mice, while Runx2 ablation in chondrocytes largely reverses OA lesions caused
432 by Kindlin-2 deletion without down-regulating p-Stat3 in chondrocytes.

433 Our results of the present study suggest that Kindlin-2 deficiency activates Stat3 by
434 at least in part stimulation of ROS overproduction in chondrocytes. Kindlin-2 deletion
435 results in overproduction of ROS in chondrocyte in vitro and in cartilage. The levels of
436 mitochondrial ROS are also elevated in articular chondrocytes in mouse and human OA
437 cartilage samples. H_2O_2 increases the level of p-Stat3 in ATDC5 cells. The ROS
438 scavenger NAC blocks Stat3 activation and up-regulation of Runx2 and ECM-degrading
439 enzymes caused by Kindlin-2 knockdown. Studies from literature also point to a link
440 between excessive mitochondrial ROS accumulation and OA pathogenesis (*49*). While
441 these observations suggest that Kindlin-2 deficiency causes OA partially through up-
442 regulation of ROS in chondrocytes, how Kindlin-2 loss promotes mitochondrial ROS
443 accumulation in chondrocytes remains unclear. It is known that mitochondrion is the
444 primary source for intracellular ROS (*46*). We find that a significant fraction of Kindlin-2

bioRxiv preprint doi: https://doi.org/10.1101/2021.08.11.456023; this version posted August 12, 2021. The copyright holder for this preprint (which was not certified by peer review) is the author/funder. All rights reserved. No reuse allowed without permission.

445 protein exists in mitochondrion of chondrocytes. Our recently published study showed
446 that Kindlin-2 is detected in mitochondrion of lung cancer cells (*34*). A more recent study
447 revealed that suppression of Kindlin-2 mitochondrial translocation and its interaction with
448 pyrroline-5-carboxylate reductase 1 by deletion of Pinch1, another focal adhesion protein,
449 resulted in ROS overaccumulation in lung adenocarcinoma cells (*35*). In addition to Stat3
450 activation, the loss of Kindlin-2 also promotes Stat3 nuclear translocation in chondrocytes
451 with possible mechanism involving interactions of both factors.

452 Interestingly, systemic inhibition or genetic deletion of Stat3 in chondrocytes
453 attenuates the cartilage loss and osteophyte outgrowth, but not the synovial hyperplasia,
454 caused by Kindlin-2 deficiency. This suggests that Kindlin-2 deficiency causes synovial
455 hyperplasia not through activation of Stat3. It should be noted that the expression levels
456 of Kindlin-2 protein are comparable in synoviums of control and cKO mice. This is
457 consistent with the fact that *Aggrecan*^{CreERT2} is not active in the synovium (Supplementary
458 Figure 2a) (*50*). Thus, the synovial hyperplasia observed in cKO mice is not due to Kindlin-
459 2 deficiency in this tissue.

460 Loss of β1 integrin activation was reported to disturb chondrocyte cytokinesis,
461 motility and survival, leading to accelerated terminal differentiation of articular
462 chondrocytes (*51*)(*52*). In the present study, we find that loss of Kindlin-2 impairs β1
463 integrin activation in articular chondrocytes without activating the MAPK pathway. This
464 result is consistent with a previous report showing a normal MAPK activation in β1
465 integrin-deficient chondrocytes (*52*). In this study, we demonstrate that deletion of Kindlin-
466 2 impairs the attachment and spreading of articular chondrocytes on collagen II coated
467 surfaces. Thus, impaired activation of β1 integrin could partially contribute to the
468 enhanced chondrocyte hypertrophic differentiation and catabolism as well as OA lesions
469 in cKO mice.

470 It is worthwhile to point out that the spontaneous OA mouse model generated by
471 inducible deletion of Kindlin-2 in adult mice developed in this study is an invaluable tool
472 for OA study in the field. After TM injection, cKO mice develop spontaneous OA

bioRxiv preprint doi: https://doi.org/10.1101/2021.08.11.456023; this version posted August 12, 2021. The copyright holder for this preprint (which was not certified by peer review) is the author/funder. All rights reserved. No reuse allowed without permission.

473 phenotypes over time with a 100% penetration (with greater than 100 mice). More
474 importantly, the OA phenotypes highly photocopy those of human OA, including
475 progressive cartilage degeneration, osteophyte formation, synovial hyperplasia and pain.
476 Another advantage of this spontaneous OA mouse model over the DMM OA model is that
477 the former takes a slower process to induce OA initiation, development and progression,
478 which is similar to the pathological process of human OA, a chronic degenerative disease.
479 Furthermore, this model avoids the trouble of the DMM surgery; the latter also creates
480 greater experimental variations.

481 A large number of elderly people suffer from OA worldwide. However, there are
482 currently no FDA-approved OA treatments or effective interventions to limit OA
483 development and progression. The pathway comprising of Kindlin-2, Stat3 and Runx2
484 defined in this study may be a useful target for the intervention and treatment of OA.
485 Notably, we provide convincing evidence that intraarticular injection of Kindlin-2-
486 expressing AAV limits progression of aging- and instability-induced OA in mice.

487 We acknowledge that this study has several limitations. First, while our results show
488 significant limitation of both aging- and instability-induced OA lesions by a single
489 intracellular injection of Kindlin-2 AAV5 in mice, its long-term protective effect against OA
490 remains unclear. This needs to be determined by performing time-course experiments. If
491 the effect of single injection turns out to be unsustainable, we will need to determine
492 whether multiple injections and/or reformulation, for example, by slow release methods,
493 can extend the effectiveness of treatment. Second, in this study, we did not determine
494 whether this injection regimen of AAV-Kindlin-2 will have a similar protective effect against
495 OA development and progression in primates or humans. We plan to perform these
496 experiments on primates in our future study. Third, while expression of Kindlin-2 in
497 articular chondrocytes is down-regulated in mouse and human OA cartilage samples,
498 upstream factors responsible for this down-regulation remain to be determined in future
499 study. Collectively, Kindlin-2 plays a central role in maintaining articular chondrocyte
500 homeostasis and preserving integrity of the articular cartilage and provides a protection

bioRxiv preprint doi: https://doi.org/10.1101/2021.08.11.456023; this version posted August 12, 2021. The copyright holder for this preprint (which was not certified by peer review) is the author/funder. All rights reserved. No reuse allowed without permission.

501 against OA.

bioRxiv preprint doi: https://doi.org/10.1101/2021.08.11.456023; this version posted August 12, 2021. The copyright holder for this preprint (which was not certified by peer review) is the author/funder. All rights reserved. No reuse allowed without permission.

Materials and Methods

Human cartilage samples

Human knee joint cartilage samples were collected from OA patients from the total joint replacement surgeries, following informed written patient consent with approval from The Ethics Committee of Tongji Medical College, Huazhong University of Science and Technology (No. [2020](*43, 44, 53*) IEC-J (565)). Cartilages were excised from tibial plateau and femoral condyles of 8 patients undergoing total knee replacement surgery. Cartilage samples were fixed in 4% paraformaldehyde, decalcified in 15% EDTA and paraffin embedded for further histological and immunofluorescent (IF) analysis.

Animal studies

Generation of *Kindlin-2*$^{fl/fl}$ mice was described (*41*). The *Aggrecan*^{CreERT2} mice and floxed Runx2 mice (*Runx2* $^{fl/fl}$) were described (*50, 54*). Floxed Stat3 mice (*Stat3*$^{fl/fl}$)(*55*) were kindly provided by Dr. Xin-Yuan Fu of Indiana University School of Medicine. We bred *Kindlin-2*$^{fl/fl}$ mice with the *Aggrecan*^{CreERT2} knock-in mice to generate the inducible conditional Kindlin-2 knockout mice (*Kindlin-2*$^{fl/fl}$*; Aggrecan*^{CreERT2}). To delete Kindlin-2 expression, mice were administrated with five daily peritoneal injections of tamoxifen (TM, Sigma T5648) at the dosage 100 mg/kg body weight. This TM regimen dramatically reduced Kindlin-2 protein expression in knee joint articular chondrocytes (Figure 2h). *Kindlin-2*$^{fl/fl}$*; Aggrecan-*$^{Cre/ERT2}$ mice treated with corn oil were used as control groups in this study. We crossed the *K2*$^{fl/fl}$*; Aggrecan*^{CreERT2} (cKO) mice with either floxed Stat3 mice (*Stat3*$^{fl/fl}$) or floxed Runx2 mice (*Runx2*$^{fl/fl}$) to generate *K2*$^{fl/fl}$*; Stat3*$^{fl/fl}$*; Aggrecan*^{CreERT2} mice (^{KS}dKO) and *K2*$^{fl/fl}$*; Runx2*$^{fl/fl}$*; Aggrecan*^{CreERT2} mice (^{KR}dKO), respectively. The intraarticular injection of AAV was performed as we previously described (*11*). DMM surgery was performed in the right knees of mice for OA induction according to our previously established protocol (*56*). To minimize use of animals, only male mice were used for experiments in this study. Mice with a C57BL/6 genetic background were used for the experiments in this study. All research protocols in this study were approved by

bioRxiv preprint doi: https://doi.org/10.1101/2021.08.11.456023; this version posted August 12, 2021. The copyright holder for this preprint (which was not certified by peer review) is the author/funder. All rights reserved. No reuse allowed without permission.

530 the Institutional Animal Care and Use Committees (IACUC) of Southern University of
531 Science and Technology.
532

533 **Micro-computerized tomography**

534 Knee joints were subjected to micro-computerized tomography (μCT) according to our
535 previously established protocol (*11*). Briefly, we used a Skyscan scanner 1276 high-
536 resolution μCT scanner (Bruker, Aartselaar, Belgium) with 60 kVp source and 100 μAmp
537 current for formalin-fixed mouse knee joints with a resolution of 10 μm. The scanned
538 images from each group were evaluated at the same thresholds to allow three-
539 dimensional structural rendering of each sample.
540

541 **Animal behavioral tests**

542 Testing for mechanical allodynia (von Frey sensitivity) was performed essentially
543 according to a method previously described (*57*) Before the von Frey test, we allowed
544 animals to adapt to the environment, including an elevated mesh platform for 15 minutes.
545 A calibrated set of von Frey filaments (Stoelting, Wood Dale, IL) was used to poke from
546 below to the hind paw to calculate the 50% force withdrawal threshold using an iterative
547 approach. The tests were performed in a blind manner that the investigator is not aware
548 of the identification of animals as well as the study groups.
549

550 **Isolation of primary articular chondrocytes**

551 The isolation and culture of primary chondrocytes from adult articular cartilage were
552 modified from a previously described protocol (*58*). Two-month-old male mice were
553 sacrificed and the hindlimbs were dissected. The hindlimbs were washed three times with
554 PBS and then skin and soft tissues were removed from bones using scissors and pincer
555 in a sterile flow hood. Articular cartilages on femoral condyles and tibial plateau were
556 peeled off using a blunt-ended forceps and surrounding synovial layer and tendons were
557 carefully removed under a stereo microscope. Then, the isolated cartilage was crushed

bioRxiv preprint doi: https://doi.org/10.1101/2021.08.11.456023; this version posted August 12, 2021. The copyright holder for this preprint (which was not certified by peer review) is the author/funder. All rights reserved. No reuse allowed without permission.

558 into small pieces and digested in 0.25% trypsin-EDTA solution for 20 mins, followed by
559 an overnight digestion in collagenase II solution (1mg/ml). The released cells from
560 cartilage pieces were washed by PBS and cultured in 60 mm plates with Dulbecco's
561 Modified Eagle Medium/F12 medium supplemented with 10% fetal bovine serum, 1%
562 glutamine and 1% penicillin and streptomycin at 37°C with 5% CO_2 for further in vitro
563 experiments. To induce deletion of Kindlin-2 in primary articular chondrocytes of *Kindlin-*
564 *2$^{fl/fl}$; Aggrecan^{CreERT2}* mice in vitro, 4-Hydroxytamoxifen Ready Made Solution (Sigma,
565 SML1666) was added into the culture medium (1:1000) for 48 hours. Vehicle (Ethanol:
566 isopropanol (95:5)) was used as control. The expression levels of Kindlin-2, Stat3, p-Stat3
567 and Runx2 were analyzed by western blotting and IF staining.
568

569 **siRNA knockdown experiments**
570 ATDC5 cells were transfected with the indicated siRNAs. 48h after transfection, protein
571 extracts were isolated from cells and subjected to western blot analyses with indicated
572 antibodies. The sequences of siRNA primers used in this study are summarized in
573 Supplementary Table 1.
574

575 **Isolation of mitochondrial and cytosolic fractions**
576 Mitochondrial and cytosolic fractions were isolated using a Mitochondria Isolation Kit
577 (Thermo Fisher Scientific, Cat #898874) according to our previously established protocol
578 (*34*). Briefly, cultured primary articular chondrocytes were harvested by centrifuge at 850g
579 for 2 minutes and resuspended in a 2.0-ml microcentrifuge tube. Then, Reagent A, B and
580 C was sequentially added to the cells according to manufacturer's instructions. The cells
581 were centrifuged at 700g for 10 minutes at 4°C to remove the nuclei. The supernatants
582 were further centrifuged at 12,000g for 15 minutes at 4°C and then the supernatants
583 (cytosolic fractions) and pellets (mitochondrial fractions) were collected.
584
585

bioRxiv preprint doi: https://doi.org/10.1101/2021.08.11.456023; this version posted August 12, 2021. The copyright holder for this preprint (which was not certified by peer review) is the author/funder. All rights reserved. No reuse allowed without permission.

586 **Measurement of ROS**

587 The measurement of ROS in homogenized articular cartilage was performed using a 6-
588 chloromethyl-2‘,7’-dichlorodihydrofluorescein diacetate, acetyl ester; (CM-H_2DCFDA)-
589 based commercial kit (GENMED, GMS10016.3). Briefly, articular cartilages were isolated
590 from the hindlimbs of mice and homogenized using BioPulverizer system (Cat# 59012N).
591 The protein concentrations of homogenized tissues were determined using Pierce™ BCA
592 Protein Assay Kit (Thermo Fisher, Cat# 23225). The homogenized tissues were then
593 incubated with CM-H_2DCFDA probe at 37 °C for 20 min with protection from light. The
594 fluorescence intensity was measured and analyzed by EnSpire system (PerkinElmer).
595 The relative fluorescence intensity was taken as the average values from three repeated
596 experiments. The mitochondrial ROS levels were measured using the MitoSOX red
597 Mitochondrial Superoxide Indicator (Thermo Fisher, Cat# M36008) following the
598 manufacturer's instruction. The MitoSOX reagents were prepared at a 5 μM working
599 concentration in HBSS/Ca/Mg buffer. For the detection of mitochondrial ROS in cultured
600 cells, cells were washed 3 times by PBS and then loaded with 5 μM MitoSOX reagent
601 and incubated at 37 °C for 10 min under protection of light. For the measurement of ROS
602 levels in articular cartilage, paraformaldehyde-fixed, sections (5 μm) were incubated with
603 5 μM MitoSOX Red for 15 min at room temperature under protection of light as previously
604 described (*59, 60*). Nuclei were stained with DAPI. the fluorescence signals were
605 analyzed by SP8 Leica confocal microscopy (excitation wavelength 510 nm, emission
606 wavelength 580 nm). Human cartilage samples were fixed in Methacarn fixative solution
607 (10% glacial acetic acid, 30% trichloromethane and 60% methanol) at 4 °C overnight and
608 decalcified in 15% EDTA (without PFA) in PBS. OxyIHC staining was performed according
609 the Millipore OxyIHCTM oxidative stress detection kit protocol (Millipore, S7450).

610

611 **RNA sequencing analysis**

612 Total RNA was extracted from homogenized articular cartilage tissues of control and cKO
613 mice at 5 months after TM injections using a TransZol Up Plus RNA Kit (ER501-01;

bioRxiv preprint doi: https://doi.org/10.1101/2021.08.11.456023; this version posted August 12, 2021. The copyright holder for this preprint (which was not certified by peer review) is the author/funder. All rights reserved. No reuse allowed without permission.

614 Transgen, China) and 3 μg RNA per sample was used as input material for the RNA
615 sample preparations. Sequencing libraries were generated using NEBNext R UltraTM
616 RNA Library Prep Kit (Illunina, NEB, United States) and the library quality was assessed
617 on the Agilent Bioanalyzer 2100 system. After cluster generation, the library preparations
618 were sequenced on an Illumina Hiseq platform and 150 bp paired-end reads were
619 generated. After quality control, reads mapping to the reference genome and
620 quantification of gene expression level, KEGG enrichment analyses were performed by
621 using the cluster Profiler R package.

622

623 **Western blot analyses**

624 Western blot analysis was performed as previously described (*61*). Briefly, protein
625 extracts were fractionated on a 10% SDS-PAGE gel and transferred onto nitrocellulose
626 membranes (Schleicher & Schuell, Keene, NH). The membrane was blocked in 5% nonfat
627 milk in Tris-buffered saline/Tween 20 buffer and probed with primary antibodies, followed
628 by incubation with secondary antibodies conjugated with horseradish peroxidase, and
629 then visualized using a Western Blotting Detection Kit (GE Healthcare, cat#: RPN2106).
630 Antibodies used in this study are listed in Supplementary Table 2.

631

632 **Histology, immunofluorescence and confocal analysis**

633 Knee joint tissues were fixed in 4% paraformaldehyde, decalcified, dehydrated, and
634 embedded in paraffin. Serial sections (5-μm thick) were cut and stained with Safranin O
635 & Fast Green (Solarbio, Cat#G1371)/hematoxylin and eosin (Thermo Fisher
636 Cat#7211&7111) for morphological analysis according to manufacturer's instructions. For
637 IF staining, 5-μm sections were permeabilized with 0.2% Triton X-100, blocked with 2%
638 bovine serum albumin (BSA) for 1h and then incubated with primary antibodies
639 (Supplemental Table 2) overnight at 4°C. After washing, the sections were incubated with
640 anti-rabbit Alexa Fluor 488 (Invitrogen) or anti-mouse Alexa Fluor 568 (Invitrogen)
641 secondary antibodies (1:400) for 1h at room temperature. The fluorescent signals in

bioRxiv preprint doi: https://doi.org/10.1101/2021.08.11.456023; this version posted August 12, 2021. The copyright holder for this preprint (which was not certified by peer review) is the author/funder. All rights reserved. No reuse allowed without permission.

642 articular cartilage areas were determined using a confocal microscope (Leica SP8
643 Confocal Microsystems).
644

645 **Quantitative real-time PCR analysis**

646 Total RNA was extracted from cells with TriPure Isolation Reagent (Sigma-Aldrich) as
647 previously described (*62*). Reverse transcription to cDNA was prepared by using
648 Superscript II reverse transcriptase (Invitrogen) and oligo(dT) primers. Real-time PCR
649 was performed using SYBR ® Premix Ex Taq™ II with an ABI 7500 QPCR System. Mouse
650 *Gapdh* mRNA levels were used as an internal control of the target mRNAs. Normalization
651 and fold changes were calculated using the ΔΔCt method. Primer sets are listed in
652 Supplementary Table 3.
653

654 **Statistical Analysis**

655 The sample size for each experiment was determined based on our previous experience.
656 Animals used in experiments of this study were randomly grouped. IF and histology were
657 performed and analyzed in a double-blinded way. Statistical analyses were completed
658 using the Prism GraphPad. The two-tailed unpaired Student's *t* test (two groups) and one-
659 way ANOVA (multiple groups), followed by Tukey's post-hoc test, were used. Results are
660 expressed as mean ± standard deviation (s.d.), as indicated in the Figure Legends.
661 Differences with $P < 0.05$ were considered statistically significant.
662

663 **Data availability**

664 All data generated for this study are available from the corresponding authors upon
665 reasonable request.

bioRxiv preprint doi: https://doi.org/10.1101/2021.08.11.456023; this version posted August 12, 2021. The copyright holder for this preprint (which was not certified by peer review) is the author/funder. All rights reserved. No reuse allowed without permission.

666 **References**

667 1. D. J. Hunter, S. Bierma-Zeinstra, Osteoarthritis. *Lancet* **393**, 1745-1759 (2019).
668 2. Y. He, Z. Li, P. G. Alexander, B. D. Ocasio-Nieves, L. Yocum, H. Lin, R. S. Tuan,
669 Pathogenesis of Osteoarthritis: Risk Factors, Regulatory Pathways in
670 Chondrocytes, and Experimental Models. *Biology (Basel)* **9**, (2020).
671 3. M. M. Sun, F. Beier, Chondrocyte hypertrophy in skeletal development, growth,
672 and disease. *Birth Defects Res C Embryo Today* **102**, 74-82 (2014).
673 4. D. Chen, J. Shen, W. Zhao, T. Wang, L. Han, J. L. Hamilton, H. J. Im,
674 Osteoarthritis: toward a comprehensive understanding of pathological
675 mechanism. *Bone Res* **5**, 16044 (2017).
676 5. E. K. Song, J. Jeon, D. G. Jang, H. E. Kim, H. J. Sim, K. Y. Kwon, S. Medina-
677 Ruiz, H. J. Jang, A. R. Lee, J. G. Rho, H. S. Lee, S. J. Kim, C. Y. Park, K. Myung,
678 W. Kim, T. Kwon, S. Yang, T. J. Park, ITGBL1 modulates integrin activity to
679 promote cartilage formation and protect against arthritis. *Sci Transl Med* **10**,
680 (2018).
681 6. E. Charlier, C. Deroyer, S. Neuville, Z. Plener, O. Malaise, F. Ciregia, P. Gillet, G.
682 Reuter, M. Salve, N. Withofs, R. Hustinx, D. de Seny, M. G. Malaise, Toward
683 diagnostic relevance of the alphaVbeta5, alphaVbeta3, and alphaVbeta6
684 integrins in OA: expression within human cartilage and spinal osteophytes. *Bone*
685 *Res* **8**, 35 (2020).
686 7. Q. Wang, K. Onuma, C. Liu, H. Wong, M. S. Bloom, E. E. Elliott, R. R. Cao, N.

bioRxiv preprint doi: https://doi.org/10.1101/2021.08.11.456023; this version posted August 12, 2021. The copyright holder for this preprint (which was not certified by peer review) is the author/funder. All rights reserved. No reuse allowed without permission.

687 Hu, N. Lingampalli, O. Sharpe, X. Zhao, D. H. Sohn, C. M. Lepus, J. Sokolove,
688 R. Mao, C. T. Cisar, H. Raghu, C. R. Chu, N. J. Giori, S. B. Willingham, S. S.
689 Prohaska, Z. Cheng, I. L. Weissman, W. H. Robinson, Dysregulated integrin
690 alphaVbeta3 and CD47 signaling promotes joint inflammation, cartilage
691 breakdown, and progression of osteoarthritis. *JCI Insight* **4**, (2019).
692 8. Q. Zheng, G. Zhou, R. Morello, Y. Chen, X. Garcia-Rojas, B. Lee, Type X
693 collagen gene regulation by Runx2 contributes directly to its hypertrophic
694 chondrocyte-specific expression in vivo. *J Cell Biol* **162**, 833-842 (2003).
695 9. F. Li, Y. Lu, M. Ding, D. Napierala, S. Abbassi, Y. Chen, X. Duan, S. Wang, B.
696 Lee, Q. Zheng, Runx2 contributes to murine Col10a1 gene regulation through
697 direct interaction with its cis-enhancer. *J Bone Miner Res* **26**, 2899-2910 (2011).
698 10. L. Liao, S. Zhang, J. Gu, T. Takarada, Y. Yoneda, J. Huang, L. Zhao, C. D. Oh, J.
699 Li, B. Wang, M. Wang, D. Chen, Deletion of Runx2 in Articular Chondrocytes
700 Decelerates the Progression of DMM-Induced Osteoarthritis in Adult Mice. *Sci*
701 *Rep* **7**, 2371 (2017).
702 11. J. Huang, L. Zhao, Y. Fan, L. Liao, P. X. Ma, G. Xiao, D. Chen, The microRNAs
703 miR-204 and miR-211 maintain joint homeostasis and protect against
704 osteoarthritis progression. *Nat Commun* **10**, 2876 (2019).
705 12. S. E. Catheline, D. Hoak, M. Chang, J. P. Ketz, M. J. Hilton, M. J. Zuscik, J. H.
706 Jonason, Chondrocyte-Specific RUNX2 Overexpression Accelerates Post-
707 traumatic Osteoarthritis Progression in Adult Mice. *J Bone Miner Res* **34**, 1676-

bioRxiv preprint doi: https://doi.org/10.1101/2021.08.11.456023; this version posted August 12, 2021. The copyright holder for this preprint (which was not certified by peer review) is the author/funder. All rights reserved. No reuse allowed without permission.

708 1689 (2019).

709 13. S. J. Rice, G. Aubourg, A. K. Sorial, D. Almarza, M. Tselepi, D. J. Deehan, L. N.
710 Reynard, J. Loughlin, Identification of a novel, methylation-dependent, RUNX2
711 regulatory region associated with osteoarthritis risk. *Hum Mol Genet* **27**, 3464-
712 3474 (2018).

713 14. D. Chen, D. J. Kim, J. Shen, Z. Zou, R. J. O'Keefe, Runx2 plays a central role in
714 Osteoarthritis development. *J Orthop Translat* **23**, 132-139 (2020).

715 15. A. Latourte, C. Cherifi, J. Maillet, H. K. Ea, W. Bouaziz, T. Funck-Brentano, M.
716 Cohen-Solal, E. Hay, P. Richette, Systemic inhibition of IL-6/Stat3 signalling
717 protects against experimental osteoarthritis. *Ann Rheum Dis* **76**, 748-755 (2017).

718 16. S. W. Wang, Y. M. Sun, The IL-6/JAK/STAT3 pathway: potential therapeutic
719 strategies in treating colorectal cancer (Review). *Int J Oncol* **44**, 1032-1040
720 (2014).

721 17. S. Miscia, M. Marchisio, A. Grilli, V. Di Valerio, L. Centurione, G. Sabatino, F.
722 Garaci, G. Zauli, E. Bonvini, A. Di Baldassarre, Tumor necrosis factor alpha
723 (TNF-alpha) activates Jak1/Stat3-Stat5B signaling through TNFR-1 in human B
724 cells. *Cell Growth Differ* **13**, 13-18 (2002).

725 18. Y. A. Kadry, D. A. Calderwood, Chapter 22: Structural and signaling functions of
726 integrins. *Biochim Biophys Acta Biomembr* **1862**, 183206 (2020).

727 19. Z. Sun, M. Costell, R. Fassler, Integrin activation by talin, kindlin and mechanical
728 forces. *Nat Cell Biol* **21**, 25-31 (2019).

bioRxiv preprint doi: https://doi.org/10.1101/2021.08.11.456023; this version posted August 12, 2021. The copyright holder for this preprint (which was not certified by peer review) is the author/funder. All rights reserved. No reuse allowed without permission.

729 20. M. Michael, M. Parsons, New perspectives on integrin-dependent adhesions.
730 *Curr Opin Cell Biol* **63**, 31-37 (2020).
731 21. E. Rognoni, R. Ruppert, R. Fassler, The kindlin family: functions, signaling
732 properties and implications for human disease. *J Cell Sci* **129**, 17-27 (2016).
733 22. E. F. Plow, J. Qin, The Kindlin Family of Adapter Proteins. *Circ Res* **124**, 202-204
734 (2019).
735 23. L. Svensson, K. Howarth, A. McDowall, I. Patzak, R. Evans, S. Ussar, M. Moser,
736 A. Metin, M. Fried, I. Tomlinson, N. Hogg, Leukocyte adhesion deficiency-III is
737 caused by mutations in KINDLIN3 affecting integrin activation. *Nat Med* **15**, 306-
738 312 (2009).
739 24. M. Moser, B. Nieswandt, S. Ussar, M. Pozgajova, R. Fassler, Kindlin-3 is
740 essential for integrin activation and platelet aggregation. *Nat Med* **14**, 325-330
741 (2008).
742 25. S. Schmidt, I. Nakchbandi, R. Ruppert, N. Kawelke, M. W. Hess, K. Pfaller, P.
743 Jurdic, R. Fassler, M. Moser, Kindlin-3-mediated signaling from multiple integrin
744 classes is required for osteoclast-mediated bone resorption. *J Cell Biol* **192**, 883-
745 897 (2011).
746 26. N. L. Malinin, L. Zhang, J. Choi, A. Ciocea, O. Razorenova, Y. Q. Ma, E. A.
747 Podrez, M. Tosi, D. P. Lennon, A. I. Caplan, S. B. Shurin, E. F. Plow, T. V. Byzova,
748 A point mutation in KINDLIN3 ablates activation of three integrin subfamilies in
749 humans. *Nat Med* **15**, 313-318 (2009).

bioRxiv preprint doi: https://doi.org/10.1101/2021.08.11.456023; this version posted August 12, 2021. The copyright holder for this preprint (which was not certified by peer review) is the author/funder. All rights reserved. No reuse allowed without permission.

750 27. E. Montanez, S. Ussar, M. Schifferer, M. Bosl, R. Zent, M. Moser, R. Fassler,
751 Kindlin-2 controls bidirectional signaling of integrins. *Genes Dev* **22**, 1325-1330
752 (2008).
753 28. J. Zhan, H. Zhang, Kindlins: Roles in development and cancer progression. *Int J*
754 *Biochem Cell Biol* **98**, 93-103 (2018).
755 29. X. Wei, Y. Xia, F. Li, Y. Tang, J. Nie, Y. Liu, Z. Zhou, H. Zhang, F. F. Hou, Kindlin-2
756 Mediates Activation of TGF-beta/Smad Signaling and Renal Fibrosis. *J Am Soc*
757 *Nephrol*, (2013).
758 30. Y. Sun, C. Guo, P. Ma, Y. Lai, F. Yang, J. Cai, Z. Cheng, K. Zhang, Z. Liu, Y. Tian,
759 Y. Sheng, R. Tian, Y. Deng, G. Xiao, C. Wu, Kindlin-2 Association with Rho GDP-
760 Dissociation Inhibitor alpha Suppresses Rac1 Activation and Podocyte Injury. *J*
761 *Am Soc Nephrol* **28**, 3545-3562 (2017).
762 31. K. Zhu, Y. Lai, H. Cao, X. Bai, C. Liu, Q. Yan, L. Ma, D. Chen, G. Kanaporis, J.
763 Wang, L. Li, T. Cheng, Y. Wang, C. Wu, G. Xiao, Kindlin-2 modulates MafA and
764 beta-catenin expression to regulate beta-cell function and mass in mice. *Nat*
765 *Commun* **11**, 484 (2020).
766 32. X. Xue, S. Xue, W. Wan, J. Li, H. Shi, HIF-1alpha interacts with Kindlin-2 and
767 influences breast cancer elasticity: A study based on shear wave elastography
768 imaging. *Cancer Med* **9**, 4971-4979 (2020).
769 33. B. Guo, J. Gao, J. Zhan, H. Zhang, Kindlin-2 interacts with and stabilizes EGFR
770 and is required for EGF-induced breast cancer cell migration. *Cancer Lett* **361**,

bioRxiv preprint doi: https://doi.org/10.1101/2021.08.11.456023; this version posted August 12, 2021. The copyright holder for this preprint (which was not certified by peer review) is the author/funder. All rights reserved. No reuse allowed without permission.

771 271-281 (2015).

772 34. L. Guo, C. Cui, K. Zhang, J. Wang, Y. Wang, Y. Lu, K. Chen, J. Yuan, G. Xiao, B.
773 Tang, Y. Sun, C. Wu, Kindlin-2 links mechano-environment to proline synthesis
774 and tumor growth. *Nat Commun* **10**, 845 (2019).

775 35. L. Guo, C. Cui, J. Wang, J. Yuan, Q. Yang, P. Zhang, W. Su, R. Bao, J. Ran, C.
776 Wu, PINCH-1 regulates mitochondrial dynamics to promote proline synthesis and
777 tumor growth. *Nat Commun* **11**, 4913 (2020).

778 36. L. Qin, W. Liu, H. Cao, G. Xiao, Molecular mechanosensors in osteocytes. *Bone*
779 *Res* **8**, 23 (2020).

780 37. X. He, J. Song, Z. Cai, X. Chi, Z. Wang, D. Yang, S. Xie, J. Zhou, Y. Fu, W. Li, W.
781 Kong, J. Zhan, H. Zhang, Kindlin-2 deficiency induces fatal intestinal obstruction
782 in mice. *Theranostics* **10**, 6182-6200 (2020).

783 38. L. Qi, X. Chi, X. Zhang, X. Feng, W. Chu, S. Zhang, J. Wu, Y. Song, Y. Zhang, W.
784 Kong, Y. Yu, H. Zhang, Kindlin-2 suppresses transcription factor GATA4 through
785 interaction with SUV39H1 to attenuate hypertrophy. *Cell Death Dis* **10**, 890
786 (2019).

787 39. H. Gao, Y. Guo, Q. Yan, W. Yang, R. Li, S. Lin, X. Bai, C. Liu, D. Chen, H. Cao,
788 G. Xiao, Lipoatrophy and metabolic disturbance in mice with adipose-specific
789 deletion of kindlin-2. *JCI Insight* **4**, (2019).

790 40. Z. Zhang, Y. Mu, J. Zhang, Y. Zhou, P. Cattaneo, J. Veevers, A. K. Peter, A. M.
791 Manso, K. U. Knowlton, X. Zhou, S. M. Evans, R. S. Ross, J. Chen, Kindlin-2 Is

bioRxiv preprint doi: https://doi.org/10.1101/2021.08.11.456023; this version posted August 12, 2021. The copyright holder for this preprint (which was not certified by peer review) is the author/funder. All rights reserved. No reuse allowed without permission.

792 Essential for Preserving Integrity of the Developing Heart and Preventing
793 Ventricular Rupture. *Circulation* **139**, 1554-1556 (2019).
794 41. C. Wu, H. Jiao, Y. Lai, W. Zheng, K. Chen, H. Qu, W. Deng, P. Song, K. Zhu, H.
795 Cao, D. L. Galson, J. Fan, H. J. Im, Y. Liu, J. Chen, D. Chen, G. Xiao, Kindlin-2
796 controls TGF-beta signalling and Sox9 expression to regulate chondrogenesis.
797 *Nat Commun* **6**, 7531 (2015).
798 42. H. Cao, Q. Yan, D. Wang, Y. Lai, B. Zhou, Q. Zhang, W. Jin, S. Lin, Y. Lei, L. Ma,
799 Y. Guo, Y. Wang, Y. Wang, X. Bai, C. Liu, J. Q. Feng, C. Wu, D. Chen, X. Cao, G.
800 Xiao, Focal adhesion protein Kindlin-2 regulates bone homeostasis in mice. *Bone*
801 *Res* **8**, 2 (2020).
802 43. L. Qin, X. Fu, J. Ma, M. Lin, P. Zhang, Y. Wang, Q. Yan, C. Tao, W. Liu, B. Tang,
803 D. Chen, X. Bai, H. Cao, G. Xiao, Kindlin-2 mediates mechanotransduction in
804 bone by regulating expression of Sclerostin in osteocytes. *Commun Biol* **4**, 402
805 (2021).
806 44. X. Fu, B. Zhou, Q. Yan, C. Tao, L. Qin, X. Wu, S. Lin, S. Chen, Y. Lai, X. Zou, Z.
807 Shao, M. Wang, D. Chen, W. Jin, Y. Song, H. Cao, G. Zhang, G. Xiao, Kindlin-2
808 regulates skeletal homeostasis by modulating PTH1R in mice. *Signal Transduct*
809 *Target Ther* **5**, 297 (2020).
810 45. G. Dalagiorgou, C. Piperi, C. Adamopoulos, U. Georgopoulou, A. N. Gargalionis,
811 A. Spyropoulou, I. Zoi, M. Nokhbehsaim, A. Damanaki, J. Deschner, E. K.
812 Basdra, A. G. Papavassiliou, Mechanosensor polycystin-1 potentiates

bioRxiv preprint doi: https://doi.org/10.1101/2021.08.11.456023; this version posted August 12, 2021. The copyright holder for this preprint (which was not certified by peer review) is the author/funder. All rights reserved. No reuse allowed without permission.

813 differentiation of human osteoblastic cells by upregulating Runx2 expression via
814 induction of JAK2/STAT3 signaling axis. *Cell Mol Life Sci* **74**, 921-936 (2017).
815 46. M. P. Murphy, How mitochondria produce reactive oxygen species. *Biochem J*
816 **417**, 1-13 (2009).
817 47. S. Perez-Garcia, M. Carrion, R. Villanueva-Romero, T. Hermida-Gomez, M.
818 Fernandez-Moreno, M. Mellado, F. J. Blanco, Y. Juarranz, R. P. Gomariz, Wnt
819 and RUNX2 mediate cartilage breakdown by osteoarthritis synovial fibroblast-
820 derived ADAMTS-7 and -12. *J Cell Mol Med* **23**, 3974-3983 (2019).
821 48. T. Orfanidou, D. Iliopoulos, K. N. Malizos, A. Tsezou, Involvement of SOX-9 and
822 FGF-23 in RUNX-2 regulation in osteoarthritic chondrocytes. *J Cell Mol Med* **13**,
823 3186-3194 (2009).
824 49. D. Li, G. Xie, W. Wang, Reactive oxygen species: the 2-edged sword of
825 osteoarthritis. *Am J Med Sci* **344**, 486-490 (2012).
826 50. S. P. Henry, C. W. Jang, J. M. Deng, Z. Zhang, R. R. Behringer, B. de
827 Crombrugghe, Generation of aggrecan-CreERT2 knockin mice for inducible Cre
828 activity in adult cartilage. *Genesis* **47**, 805-814 (2009).
829 51. A. Aszodi, E. B. Hunziker, C. Brakebusch, R. Fassler, Beta1 integrins regulate
830 chondrocyte rotation, G1 progression, and cytokinesis. *Genes Dev* **17**, 2465-
831 2479 (2003).
832 52. A. Raducanu, E. B. Hunziker, I. Drosse, A. Aszodi, Beta1 integrin deficiency
833 results in multiple abnormalities of the knee joint. *J Biol Chem* **284**, 23780-23792

bioRxiv preprint doi: https://doi.org/10.1101/2021.08.11.456023; this version posted August 12, 2021. The copyright holder for this preprint (which was not certified by peer review) is the author/funder. All rights reserved. No reuse allowed without permission.

834 (2009).
835 53. R. T. Franceschi, P. R. Romano, K. Y. Park, Regulation of type I collagen
836 synthesis by 1,25-dihydroxyvitamin D3 in human osteosarcoma cells. *J Biol*
837 *Chem* **263**, 18938-18945 (1988).
838 54. L. Liao, H. Jiang, Y. Fan, R. S. Lu, C. Wei, T. Takarada, S. He, D. Chen, Runx2 is
839 required for postnatal intervertebral disc tissue growth and development. *J Cell*
840 *Physiol* **234**, 6679-6687 (2019).
841 55. A. Moh, Y. Iwamoto, G. X. Chai, S. S. Zhang, A. Kano, D. D. Yang, W. Zhang, J.
842 Wang, J. J. Jacoby, B. Gao, R. A. Flavell, X. Y. Fu, Role of STAT3 in liver
843 regeneration: survival, DNA synthesis, inflammatory reaction and liver mass
844 recovery. *Lab Invest* **87**, 1018-1028 (2007).
845 56. J. Li, B. Zhang, W. X. Liu, K. Lu, H. Pan, T. Wang, C. D. Oh, D. Yi, J. Huang, L.
846 Zhao, G. Ning, C. Xing, G. Xiao, R. Liu-Bryan, S. Feng, D. Chen, Metformin limits
847 osteoarthritis development and progression through activation of AMPK
848 signalling. *Ann Rheum Dis* **79**, 635-645 (2020).
849 57. S. R. Chaplan, F. W. Bach, J. W. Pogrel, J. M. Chung, T. L. Yaksh, Quantitative
850 assessment of tactile allodynia in the rat paw. *J Neurosci Methods* **53**, 55-63
851 (1994).
852 58. M. Gosset, F. Berenbaum, S. Thirion, C. Jacques, Primary culture and
853 phenotyping of murine chondrocytes. *Nat Protoc* **3**, 1253-1260 (2008).
854 59. L. Valls-Lacalle, I. Barba, E. Miro-Casas, J. J. Alburquerque-Bejar, M. Ruiz-

bioRxiv preprint doi: https://doi.org/10.1101/2021.08.11.456023; this version posted August 12, 2021. The copyright holder for this preprint (which was not certified by peer review) is the author/funder. All rights reserved. No reuse allowed without permission.

855 Meana, M. Fuertes-Agudo, A. Rodriguez-Sinovas, D. Garcia-Dorado, Succinate
856 dehydrogenase inhibition with malonate during reperfusion reduces infarct size
857 by preventing mitochondrial permeability transition. *Cardiovasc Res* **109**, 374-
858 384 (2016).
859 60. C. Vaamonde-Garcia, J. Loureiro, M. N. Valcarcel-Ares, R. R. Riveiro-Naveira, O.
860 Ramil-Gomez, L. Hermida-Carballo, A. Centeno, R. Meijide-Failde, F. J. Blanco,
861 M. J. Lopez-Armada, The mitochondrial inhibitor oligomycin induces an
862 inflammatory response in the rat knee joint. *BMC Musculoskelet Disord* **18**, 254
863 (2017).
864 61. G. Xiao, D. Jiang, C. Ge, Z. Zhao, Y. Lai, H. Boules, M. Phimphilai, X. Yang, G.
865 Karsenty, R. T. Franceschi, Cooperative Interactions between Activating
866 Transcription Factor 4 and Runx2/Cbfa1 Stimulate Osteoblast-specific
867 Osteocalcin Gene Expression. *J Biol Chem* **280**, 30689-30696 (2005).
868 62. Y. Lei, X. Fu, P. Li, S. Lin, Q. Yan, Y. Lai, X. Liu, Y. Wang, X. Bai, C. Liu, D. Chen,
869 X. Zou, X. Cao, H. Cao, G. Xiao, LIM domain proteins Pinch1/2 regulate
870 chondrogenesis and bone mass in mice. *Bone Res* **8**, 37 (2020).
871
872
873

bioRxiv preprint doi: https://doi.org/10.1101/2021.08.11.456023; this version posted August 12, 2021. The copyright holder for this preprint (which was not certified by peer review) is the author/funder. All rights reserved. No reuse allowed without permission.

874 **Acknowledgments**

875 The authors acknowledge the assistance of Core Research Facilities of Southern
876 University of Science and Technology. This work was supported, in part, by the National
877 Key Research and Development Program of China Grants (2019YFA0906004), the
878 National Natural Science Foundation of China Grants (81991513, 82022047, 81630066,
879 81870532, 82972100), the Guangdong Provincial Science and Technology Innovation
880 Council Grant (2017B030301018), and the Science and Technology Innovation
881 Commission of Shenzhen Municipal Government Grants (JCYJ20180302174246105,
882 JCYJ20180302174117738 and KQJSCX20180319114434843).

883

884 **Author contributions:** Study design: GX, XW, YL and HC. Study conduct and data
885 collection: XW, YL, SC, CZ, XF, CT, JL, JH, WT, HT, XB and GX. Data analysis: XW, YL
886 and GX. Data interpretation: GX, XW, CL, ZS, XB and DC. Drafting the manuscript: GX
887 and XW. XW, HC and GX take the responsibility for the integrity of the data analysis.

888

889 **Competing Interests:** The authors declare that they have no competing financial interest.

bioRxiv preprint doi: https://doi.org/10.1101/2021.08.11.456023; this version posted August 12, 2021. The copyright holder for this preprint (which was not certified by peer review) is the author/funder. All rights reserved. No reuse allowed without permission.

890 **Figure 1. Kindlin-2 is highly expressed in chondrocyte of the hyaline articular
891 cartilage and is reduced in aged mouse and human OA cartilages.** (**a-c**) Safranin O
892 & Fast Green (SO&FG) and immunofluorescent (IF) staining of serial sections of mouse
893 (top) and human (bottom) knee joint cartilage. Green double headed arrow indicates
894 hyaline cartilage; Red double headed arrow indicates the calcified cartilage. Red dashed
895 line indicates the tide mark. Scale bar: 50 μm. Quantification of Kindlin1-, 2- and -3-
896 positive cells in articular cartilage (b,c). (**d-f**) SO&FG and IF staining of serial knee joint
897 sections from young (2-mo-old) and aged (24-mo-old) mice. Scale bar: 50 μm.
898 Quantification of Kindlin-2-positive cells in cartilage (f). (**g**) Human knee joint articular
899 cartilages were obtained from total knee replacement of OA patients. White dashed boxes
900 indicate respective normal and osteoarthritic (OA) areas. (**h**) Osteoarthritis Research
901 Society International (OARSI) score of normal and OA cartilages. (**i**) SO&FG staining of
902 normal and OA cartilages. Higher magnification images of dashed boxed areas (bottom
903 panels). Scale bar: 50 μm. Black arrowhead indicates a vertical fissure in OA cartilages.
904 (**j-o**) IF staining of normal and OA cartilage sections for expression of Kindlin-2, talin,
905 vinculin, p-FAK, Col10a1 and Mmp13. Scale bar: 50 μm. Quantitative data (k-o). Results
906 are expressed as mean ± standard deviation (s.d.). $^{*}P < 0.05$, $^{**}P < 0.01$, $^{***}P < 0.001$.
907
908 **Figure 2. Inducible deletion of Kindlin-2 in chondrocytes causes striking
909 spontaneous OA in adult mice.** (**a**) A schematic diagram illustrating the experimental
910 design. At 2 months of age, *Kindlin-2$^{fl/fl}$; Aggrecan^{CreERT2}* male mice received five daily
911 intraperitoneal injections of tamoxifen (TM) (cKO, $N = 8$) and corn oil (control, $N = 8$). Six
912 months after TM injection, mice were sacrificed, and knee joints were collected. (**b**)
913 Representative images showing enlargement of the knee joint (left panel, red dashed line),
914 excessive tibial plateau angle (middle panel, red double headed arrow) and cartilage
915 damage of femoral condyles (right panel, red arrow) in cKO mice. Higher magnification
916 images of dashed boxed areas (lower panels). (**c**) Three-dimensional (3D) reconstruction
917 from micro-computerized tomography (μCT) scans of control and cKO knee joints. Scale

bioRxiv preprint doi: https://doi.org/10.1101/2021.08.11.456023; this version posted August 12, 2021. The copyright holder for this preprint (which was not certified by peer review) is the author/funder. All rights reserved. No reuse allowed without permission.

918 bar, 1.0 mm. (**d**) The volume of calcified meniscus and synovial tissue was analyzed by
919 μCT. (**e**) von Frey test. Three months after TM injection, cKO male mice display a
920 hyperalgesia with a dramatic reduction in the 50% paw withdrawal threshold. (**f**) SO&FG
921 staining of control and cKO knee joint sections (left panel). Higher magnification images
922 showing dramatic articular cartilage loss (middle panels) and osteophyte outgrowth (right
923 panels, red arrowheads). Scale bar: 50 μm. (**g**) H&E staining of control and cKO knee
924 joint sections. Arrowheads show marked synovial hyperplasia. Scale bar: 50 μm. (**h**)
925 SO&FG and IF staining of serial knee joint sections were performed to determine
926 expression of Kindlin-2, Runx2, Col10a1 and Mmp13 in articular cartilage. Scale bar: 50
927 μm. (**i-l**) Quantification of OARSI score (i), cartilage area (j), osteophyte score (k) and
928 synovitis score (l) was performed using histological sections. (**m-p**) Quantitative data of
929 expression of Kindlin-2 (m), Runx2 (n), Cola10a1 (o) and Mmp13 (p). Results are
930 expressed as mean ± standard deviation (s.d.). $^{***}P < 0.001$.
931
932 **Figure 3. Kindlin-2 deficiency in chondrocytes accelerates OA progression in mice**
933 **with DMM surgery.** (**a**) A schematic diagram illustrating the experimental design. (**b**) μCT
934 scans of knee joints from control and cKO mice at 8 weeks after sham or DMM surgery.
935 $N = 8$ per group. Scale bar, 1.00 mm. (**c**) The volume of calcified meniscus and synovial
936 tissue was analyzed by μCT. (**d**) Representative images of SO&FG-stained sections of
937 control and cKO knee joints. Higher magnification images (right two panels) showing
938 exacerbated cartilage loss (red arrowheads) and osteophyte outgrowth (black arrows) in
939 cKO/DMM group. Scale bar: 50 μm. (**e**) Representative images of H&E staining. Scale
940 bar: 50 μm. (**f-i**) Quantification of OARSI score (f), cartilage area (g), osteophyte score (h)
941 and synovitis score (i) were performed using histological sections. Results are expressed
942 as mean ± standard deviation (s.d.). $^{*}P < 0.05$.
943
944 **Figure 4: Kindlin-2 loss induces chondrocyte hypertrophic differentiation and**
945 **catabolism through Stat3-dependent up-regulation of Runx2.** (**a**) KEGG pathway

bioRxiv preprint doi: https://doi.org/10.1101/2021.08.11.456023; this version posted August 12, 2021. The copyright holder for this preprint (which was not certified by peer review) is the author/funder. All rights reserved. No reuse allowed without permission.

946 analysis of cellular signaling pathways enriched in RNA-seq analysis using RNAs from of
947 control and cKO articular cartilages (3 mice per group) at 5 months after TM injections.
948 (**b**) ATDC5 cells were transfected with si-NC and si-K2 for 48h, followed by western
949 blotting for expression of the indicated proteins. (**c**) Quantification of (b). Experiments
950 were repeated three times independently. (**d**) IF staining of p-Stat3 in ATDC5 cells
951 transfected with si-NC and si-K2. Scale bar: 25 μm. (**e**) ATDC5 cells were transfected with
952 si-NC and si-K2 for 48h, followed by western blotting for expression of the indicated
953 proteins. (**f**) IF staining for expression of p-Stat3 in articular cartilage of control and cKO
954 mice at 3 months after TM induction. Higher magnification images of red dashed boxed
955 areas (right panels). White arrowheads indicate the elevated expression of p-Stat3 in
956 articular chondrocytes. Scale bar: 50 μm. (**g**) Quantification of (f). (**h**) Western blotting
957 analyses of expression of Kindlin-2, t-Stat3, p-Stat3 and Runx2 in articular cartilages from
958 young (2-mo) and aged (18-mo) C57BL/6 mice. (**i**) Quantification of (h). (**j**) Representative
959 images of SO&FG-stained sections of knee joints of C57BL/6 mice at different ages.
960 Higher magnification images (lower panel) showing dramatic cartilage loss (red
961 arrowheads) and osteophyte outgrowth (black arrowhead) in 18- and 24-mo-old mice.
962 Scale bar: 50 μm. (**k**) IF staining for expression of Kindlin-2, p-Stat3 and Runx2 in articular
963 cartilage of C57BL/6 mice at different ages. (**l-q**) Quantification of OARSI score (l),
964 cartilage area (m), osteophyte score (n), Kindlin-2 (o), p-Stat3 (p) and Runx2 (q) in
965 articular cartilages from C57BL/6 mice during aging. $N = 6$ per group. (**r-u**) IF staining for
966 expression of Kindlin-2, p-Stat3 and Runx2 in human normal and OA articular cartilages.
967 Scale bar: 50 μm. Quantitative data (s-u). $N = 5$ for normal, $N = 8$ for OA. (**v**) Runx2
968 knockdown. ATDC5 cells were transfected with si-NC or si-K2 with and without si-Runx2,
969 followed by western blotting. (**w**) Stat3 knockdown. ATDC5 cells were transfected with si-
970 NC or si-K2 with and without si-Stat3, followed by western blotting. All data are expressed
971 as mean ± standard deviation (s.d.) $^{*}P < 0.05$, $^{**}P < 0.01$, $^{***}P < 0.001$.
972

973 **Figure 5. Kindlin-2 deficiency promotes oxidative stress, Stat3 activation and**

bioRxiv preprint doi: https://doi.org/10.1101/2021.08.11.456023; this version posted August 12, 2021. The copyright holder for this preprint (which was not certified by peer review) is the author/funder. All rights reserved. No reuse allowed without permission.

974 **nuclear translocation in chondrocytes.** (**a**) Primary articular chondrocytes were
975 isolated from 2-month-old *Kindlin-2$^{fl/fl}$; Aggrecan^{CreERT2}* male mice. The cytosolic fraction
976 (Cyto, left lane), mitochondrial fraction (Mito, middle lane) and total cell lysates (Total,
977 right lane) of the primary chondrocytes were isolated and analyzed by western blotting
978 with antibodies against Kindlin-2, Vdac (voltage-dependent anion channel, a
979 mitochondrial marker protein) and tubulin. (**b**) The mitochondrial ROS levels in articular
980 cartilages of control and cKO mice at 3 months after TM injections were visualized by
981 MitoSOX red staining. Scale bar: 50 μm. (**c,d**) Increased level of mitochondrial ROS in
982 ATDC5 cells transfected with control (si-NC) and Kindlin-2 siRNA (si-K2) for 48h. Scale
983 bar: 25 μm. Data were quantified with 10 independent fields of view and shown in (d). (**e)**
984 Elevated ROS levels in articular cartilage extracts isolated from control and cKO mice at
985 3 months after TM induction (*N* = 8 for each group). (**f**,**g**) OxyIHC staining determining
986 the level of oxidative stress in human normal and OA articular cartilage. Quantitative data
987 were shown in (g). *N* = 5 for normal cartilages, *N* = 8 for OA cartilages. (**h**) Primary articular
988 chondrocytes were treated with the indicated concentrations of H_2O_2, followed by western
989 blotting for expression of total Stat3 (t-Stat3), phosphorylated Stat3 (p-Stat3) and Runx2.
990 (**i**) ATDC5 cells were transfected with si-NC or si-K2 with and without NAC (100 μM),
991 followed by western blotting. (**j**) Co-localization of Kindlin-2 and Stat3 in primary articular
992 chondrocytes. Scale bar, 25 μm. (**k**-**l**) Co-immunoprecipitation (co-IP) assay. COS-7 cells
993 were co-transfected with plasmids expressing Flag-Stat3 and full-length Kindlin-2. Protein
994 extracts were incubated with either Kindlin-2 antibody (k) or Flag antibody (l), followed by
995 western blotting using Flag and Kindlin-2 antibodies. (**m**) co-IP assay. Protein extracts
996 from primary articular chondrocytes were incubated with Kindlin-2 antibody or IgG,
997 followed by western blotting with antibodies against Stat3 and Kindlin-2. (**n**) ATDC5 cells
998 were transfected with empty vector (EV) and Kindlin-2 expression vector (K2). 24h later,
999 cells were treated with and without 50 μM H_2O_2 for another 12h, followed by western
1000 blotting using the indicated antibodies. (**o**) IF staining. ATDC5 cells transfected with empty
1001 vector (EV) and Kindlin-2 expression vector (K2). 24h later, cells were treated with and

bioRxiv preprint doi: https://doi.org/10.1101/2021.08.11.456023; this version posted August 12, 2021. The copyright holder for this preprint (which was not certified by peer review) is the author/funder. All rights reserved. No reuse allowed without permission.

1002 without 50 μM H_2O_2 for another 12h, followed by IF staining with p-Stat3 antibody and
1003 DAPI. Scale bar, 25 μm. (**p**) Nuclear translocation of Stat3 and K2 overexpression.
1004 ATDC5 cells transfected with empty vector (EV) and Kindlin-2 expression vector (K2). 24h
1005 later, cells were treated with and without 50 μM H_2O_2 for another 12h. Nuclear proteins
1006 and cytoplasmic proteins were separated and the expression patterns of Stat3 protein in
1007 nucleus and cytosol were detected by western blotting. PCNA (proliferating cell nuclear
1008 antigen) and Gapdh were used as control for nuclear and cytoplasmic proteins,
1009 respectively. (**q**) co-IP assay. Primary articular chondrocytes were treated with increasing
1010 concentrations of H_2O_2 for 12h and protein extracts were incubated with Kindlin-2
1011 antibody, followed by western blotting with antibodies against Stat3 and Kindlin-2.
1012
1013 **Figure 6. Genetic deletion of Stat3 in chondrocyte corrects Runx2 accumulation**
1014 **and attenuates OA lesions in cKO mice**. (**a**) A schematic diagram illustrating the
1015 experimental design. (**b**) Representative images of SO&FG-stained sections of knee
1016 joints from cKO and ^{KS}dKO mice at 10 weeks after TM injection (upper panel) or at 8
1017 weeks after DMM (lower panel). N = 8 per group. Scale bar, 50 μm. (**c**) Representative
1018 images of H&E staining. Scale bar: 50 μm. (**d**) SO&FG and IF staining of serial sections
1019 of knee joints for expression of Kindlin-2, p-Stat3, Runx2 and Col10a1 in articular cartilage
1020 of cKO and ^{KS}dKO mice. The white dashed lines indicate the articular cartilage areas.
1021 Scale bar: 50 μm. (**e-i,m-q**) Quantitative data of OARSI score (e,m), articular cartilage
1022 area (f,n), osteophyte score (g,o), synovitis score (h,p) and von Frey test (i,q). (**j-l,r-t**)
1023 Quantitative data for expression of p-Stat3 (j,r), Runx2 (k,s) and Col10a1 (l,t) in articular
1024 cartilages of cKO and ^{KS}dKO mice with or without DMM. All data are expressed as mean
1025 ± standard deviation (s.d.). $^{*}P < 0.05$, $^{**}P < 0.01$, $^{***}P < 0.001$.
1026
1027 **Figure 7. Genetical deletion of Runx2 in chondrocytes palliates spontaneous and**
1028 **DMM-induced OA defects in cKO mice.** (**a**) A schematic diagram illustrating the
1029 experimental design. (**b**) μCT scans of knee joints from cKO and ^{KR}dKO mice at 12 weeks

bioRxiv preprint doi: https://doi.org/10.1101/2021.08.11.456023; this version posted August 12, 2021. The copyright holder for this preprint (which was not certified by peer review) is the author/funder. All rights reserved. No reuse allowed without permission.

1030 after TM injection. Scale bar, 1 mm. (**c**) Representative images of Alcian Blue and Orange
1031 G (AB&OG)-stained sections of knee joints from cKO and ^{KR}dKO mice at 6 weeks (left 3
1032 panels) or at 12 weeks (right 3 panels) after TM injection. Scale bar, 50 μm. (**d**) IF staining
1033 for expression of Kindlin-2, p-Stat3 and Runx2 in cKO and ^{KR}dKO articular cartilage. The
1034 white dashed lines indicate the articular cartilage areas. Scale bar: 50 μm. (**e-g**)
1035 Quantitative data of the volume of calcified meniscus and synovial tissue (e), cartilage
1036 area (f) and von Frey test (g) at 12 weeks after TM injections. $N = 6$ mice per group. (**h**)
1037 Representative images of AB&OG-stained sections of knee joints from cKO and ^{KR}dKO
1038 mice at 8 weeks after DMM. Red arrowheads indicate articular cartilage destruction.
1039 Scale bar, 50 μm. (**i**) μCT scans of knee joints from cKO and ^{KR}dKO mice at 8 weeks after
1040 DMM. Scale bar, 1 mm. (**j-l**) Quantitative data of the volume of calcified meniscus and
1041 synovial tissue (j), cartilage area (k) and von Frey test (l) at 8 weeks after DMM. $N = 6$
1042 mice per group. All data are expressed as mean ± standard deviation (s.d.). $^{*}P < 0.05$.
1043
1044 **Figure 8. Intraarticular injection of Kindlin-2-expressing adeno-associated virus**
1045 **protects against development of aging- and DMM-induced OA in mice.** (**a**) A
1046 schematic diagram illustrating the experimental design. (**b**) GFP signals were strongly
1047 detected in articular cartilage at 3 weeks after intra-articular injection of AVV5-EGFP.
1048 Scale bar, 50 μm. (**c**) IF staining of Kindlin-2 in sham and DMM joint sections from mice
1049 intraarticularly injected with AAV5-Con (empty) or AAV5-K2. Scale bar, 50 μm. (**d**)
1050 Representative SO&FG staining images of sham and DMM joint sections (upper panels).
1051 Black dashed boxes indicate enlarged images of articular cartilage (middle panels). Red
1052 dashed boxes indicate synovium (lower panels). Scale bar: 50 μm. (**e**) Percentage of
1053 Kindlin-2-positive cells in articular cartilage. $N = 8$ per group. (**f-i**) OARSI score (f),
1054 cartilage area (g), osteophyte score (h) and synovitis score (i) were analyzed using
1055 histological sections. $N = 8$ per group. (j) Quantitative analysis of von Frey threshold (g).
1056 (**k**) Representative SO&FG-stained joint sections from aged mice intra-articular injected
1057 with AAV5-Con or AAV5-K2. Scale bar, 50 μm. (**l-p**) OARSI score (l), cartilage area (m),

bioRxiv preprint doi: https://doi.org/10.1101/2021.08.11.456023; this version posted August 12, 2021. The copyright holder for this preprint (which was not certified by peer review) is the author/funder. All rights reserved. No reuse allowed without permission.

1058 osteophyte score (n) and synovitis score (o) were analyzed. $N = 6$ per group. All data are
1059 the mean ± s.d. *$P < 0.05$, **$P < 0.01$. Student's *t*-test and one-way ANOVA with post hoc
1060 test were performed.

bioRxiv preprint doi: https://doi.org/10.1101/2021.08.11.456023; this version posted August 12, 2021. The copyright holder for this preprint (which was not certified by peer review) is the author/funder. All rights reserved. No reuse allowed without permission.

Figure 1

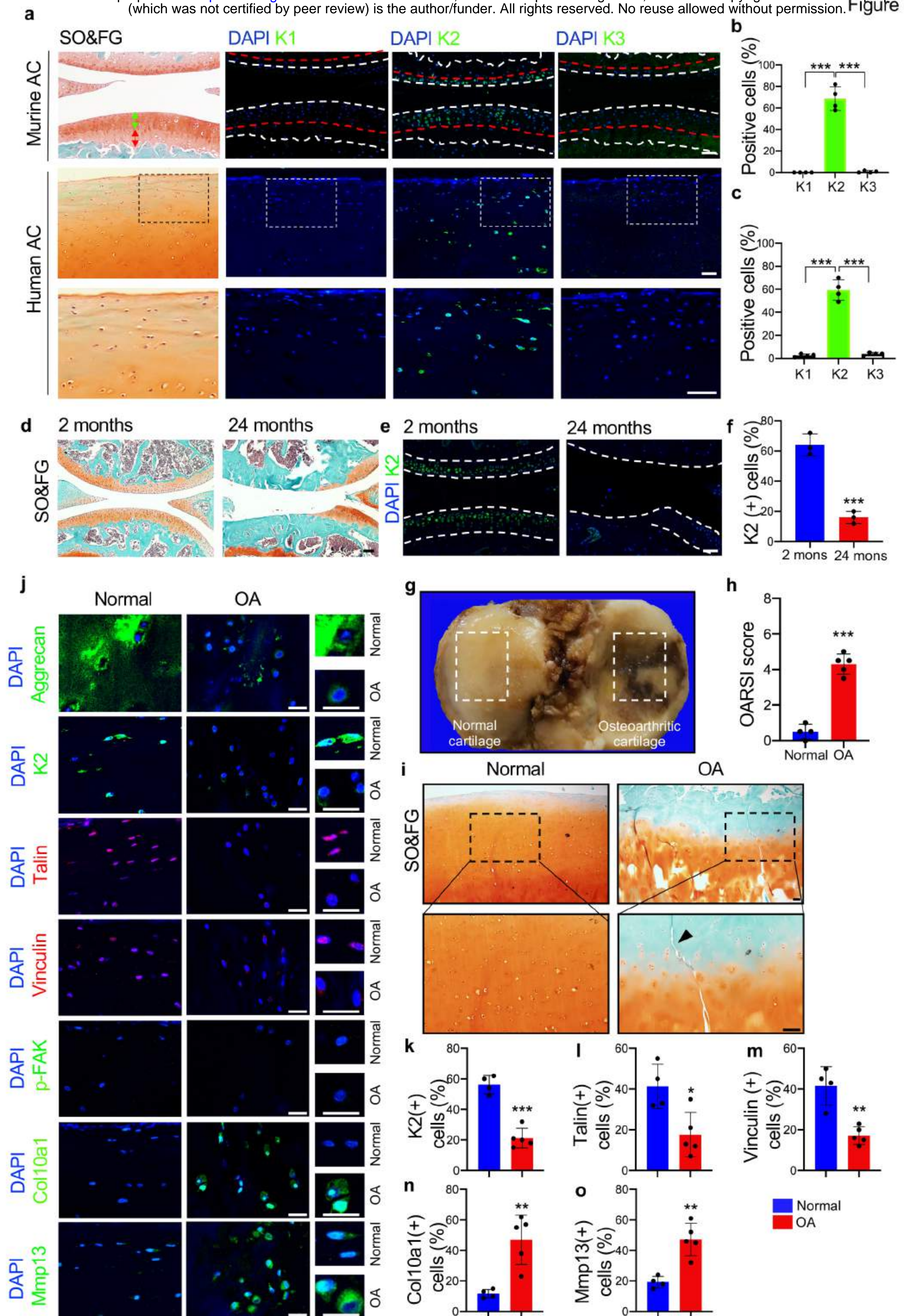

bioRxiv preprint doi: https://doi.org/10.1101/2021.08.11.456023; this version posted August 12, 2021. The copyright holder for this preprint (which was not certified by peer review) is the author/funder. All rights reserved. No reuse allowed without permission.

Figure 2

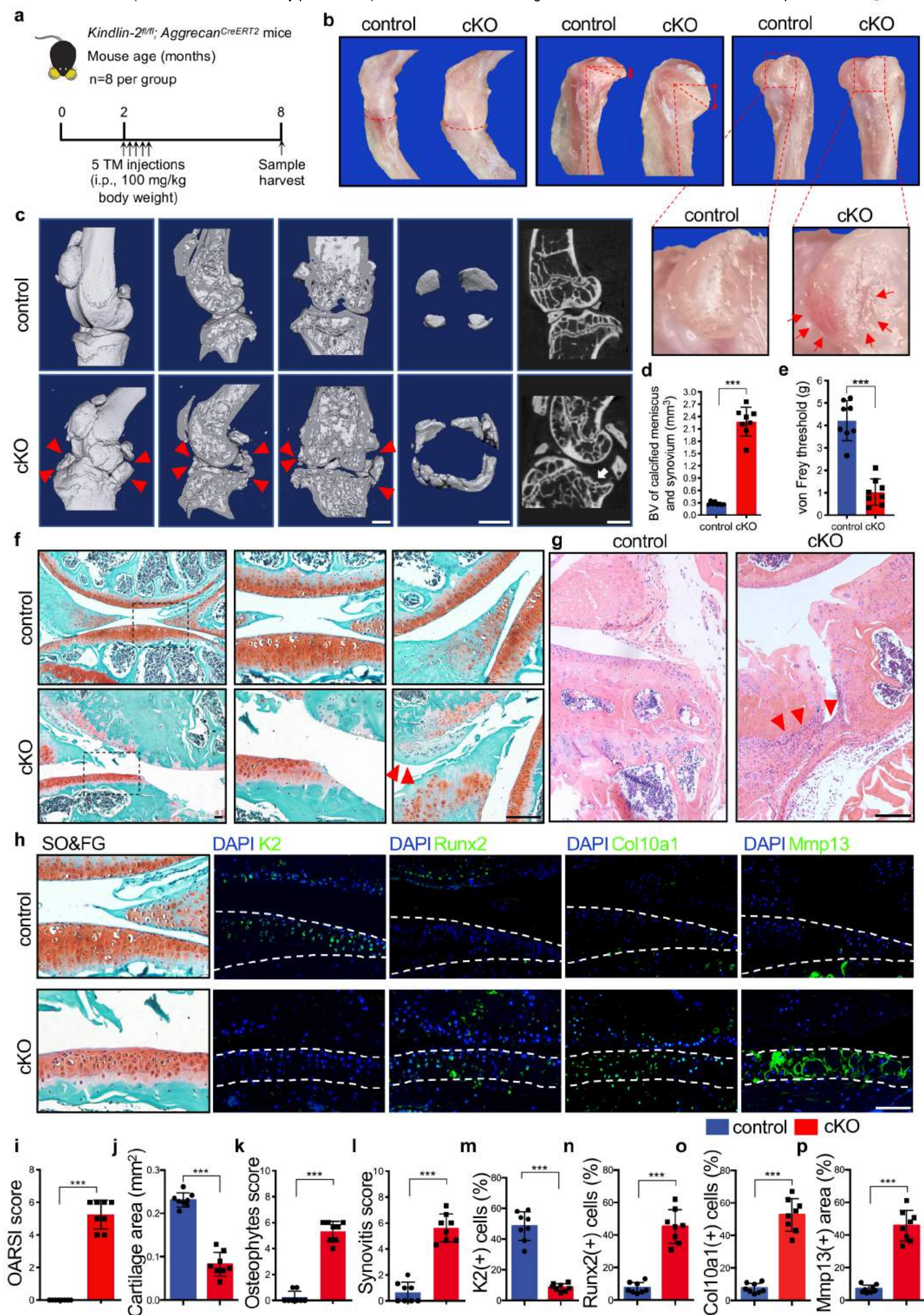

bioRxiv preprint doi: https://doi.org/10.1101/2021.08.11.456023; this version posted August 12, 2021. The copyright holder for this preprint (which was not certified by peer review) is the author/funder. All rights reserved. No reuse allowed without permission.

Figure 3

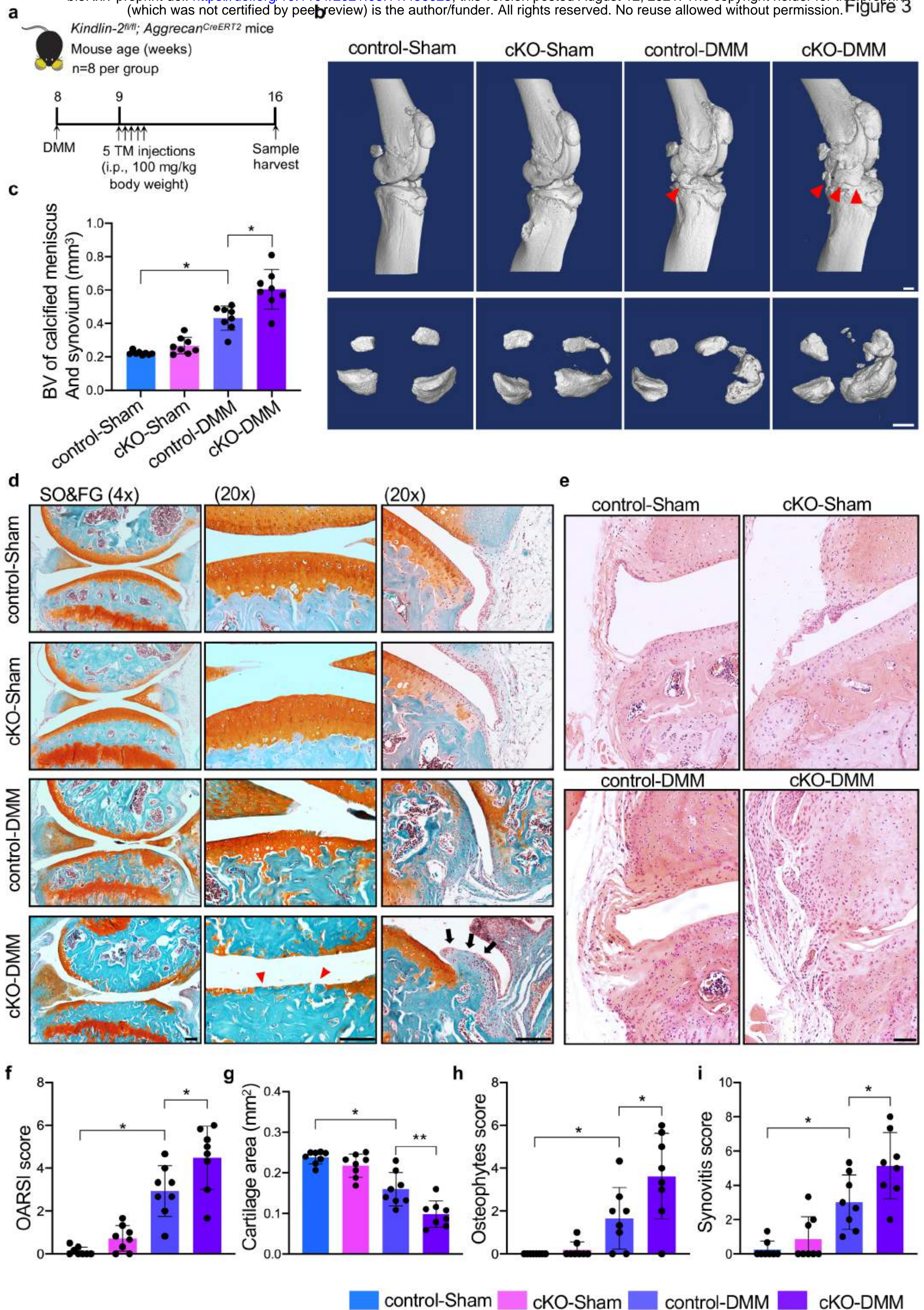

bioRxiv preprint doi: https://doi.org/10.1101/2021.08.11.456023; this version posted August 12, 2021. The copyright holder for this preprint (which was not certified by peer review) is the author/funder. All rights reserved. No reuse allowed without permission.

Figure 4

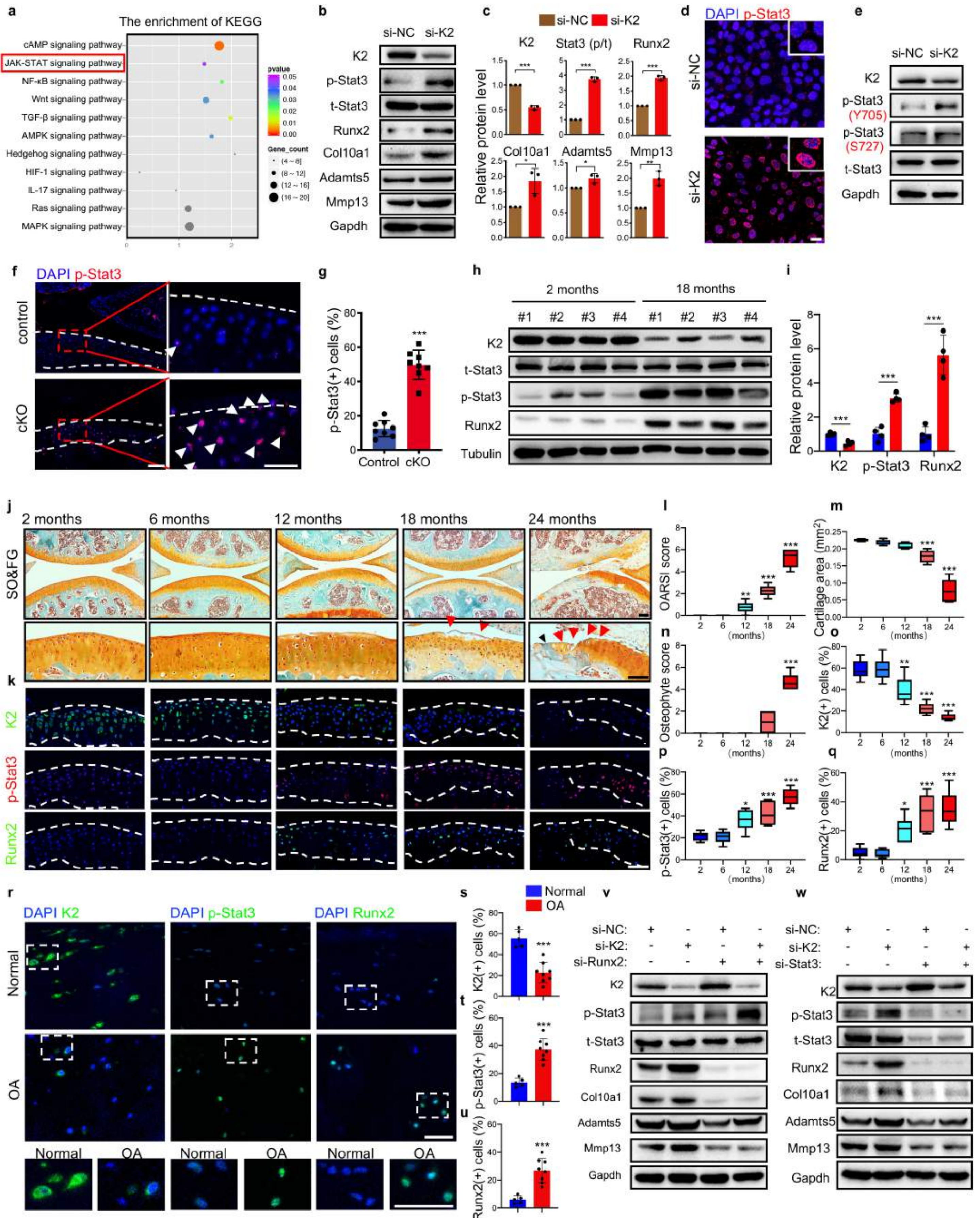

bioRxiv preprint doi: https://doi.org/10.1101/2021.08.11.456023; this version posted August 12, 2021. The copyright holder for this preprint (which was not certified by peer review) is the author/funder. All rights reserved. No reuse allowed without permission.

Figure 5

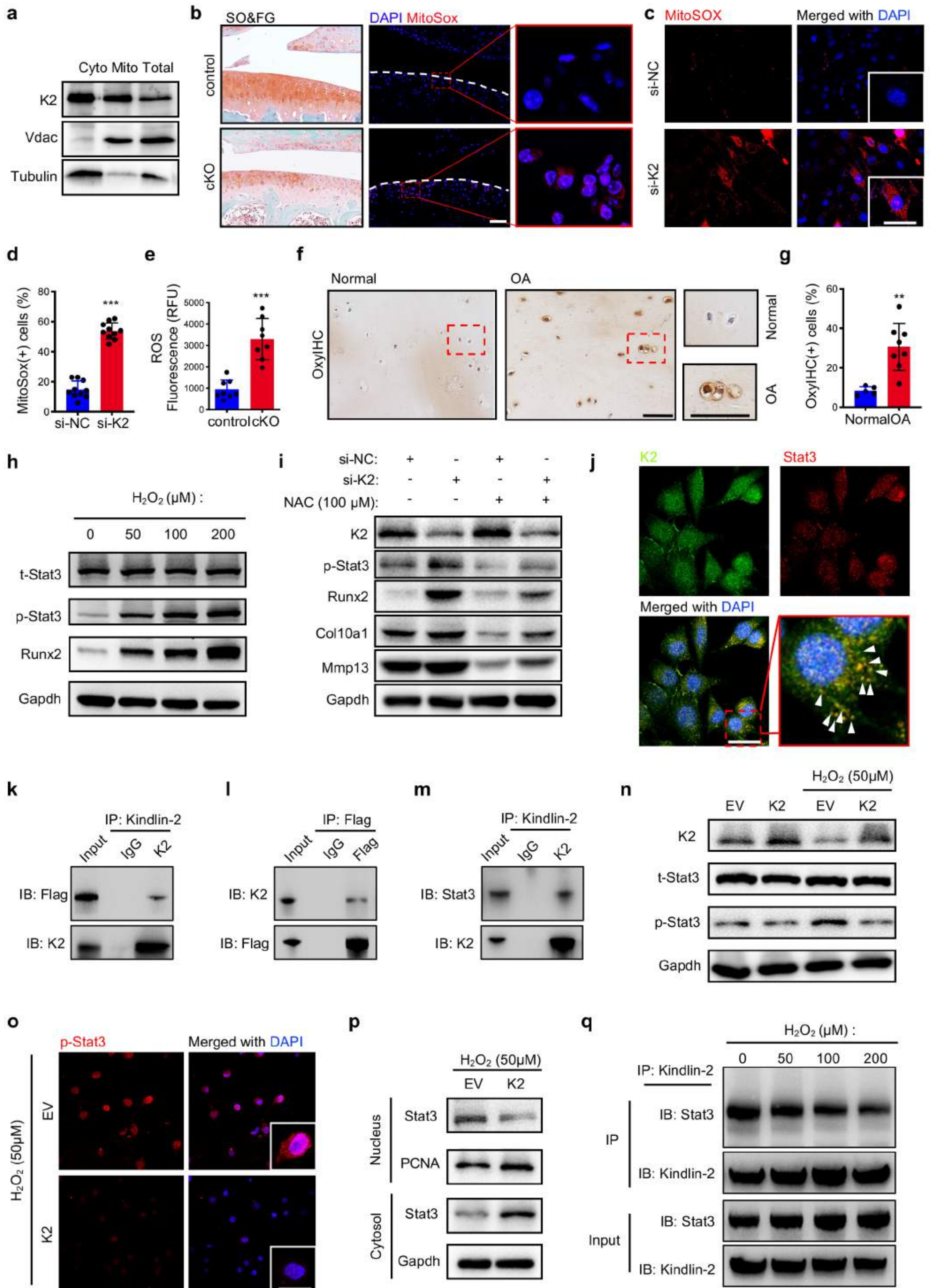

bioRxiv preprint doi: https://doi.org/10.1101/2021.08.11.456023; this version posted August 12, 2021. The copyright holder for this preprint (which was not certified by peer review) is the author/funder. All rights reserved. No reuse allowed without permission.

Figure 6

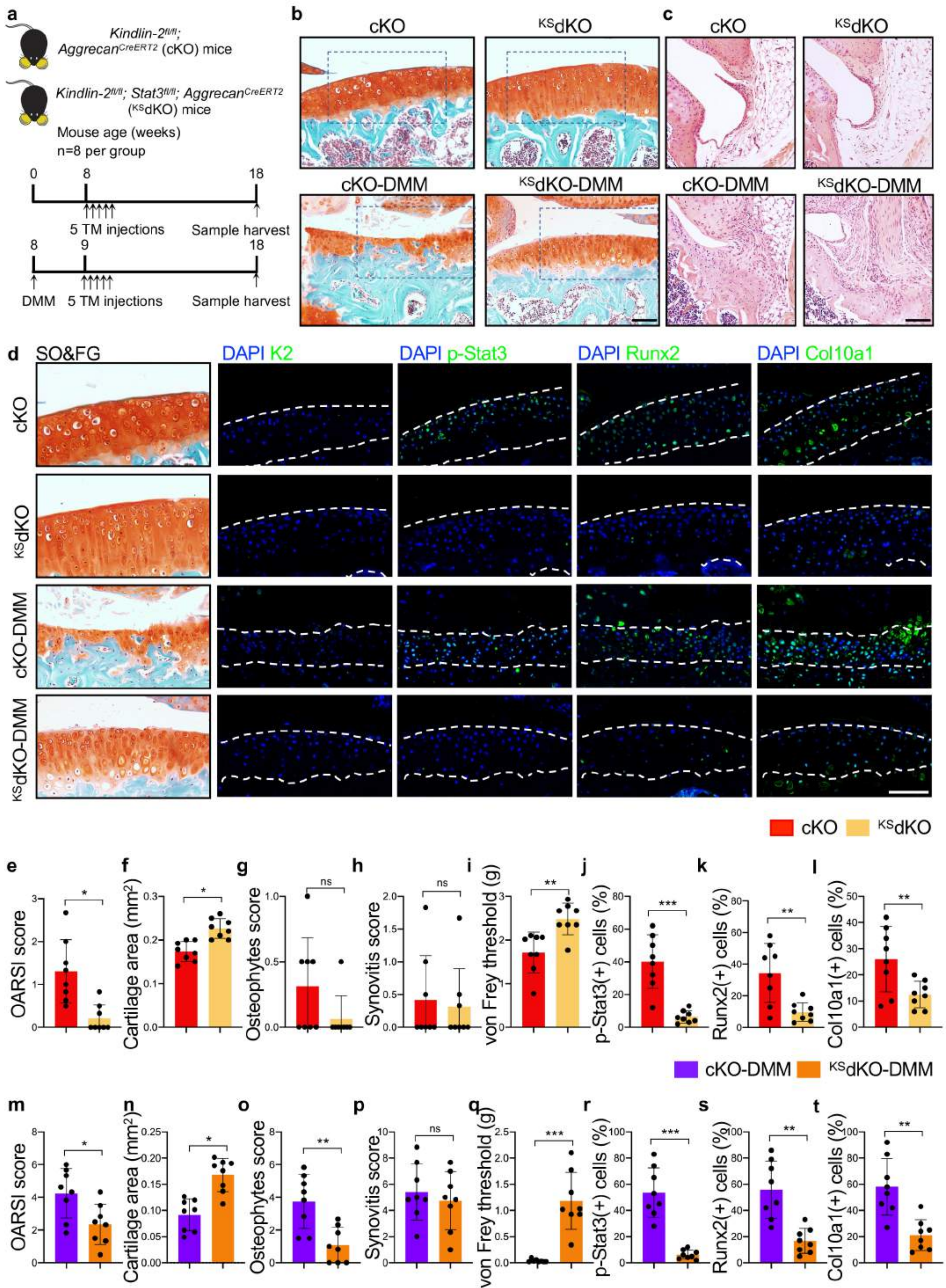

bioRxiv preprint doi: https://doi.org/10.1101/2021.08.11.456023; this version posted August 12, 2021. The copyright holder for this preprint (which was not certified by peer review) is the author/funder. All rights reserved. No reuse allowed without permission.

Figure 7

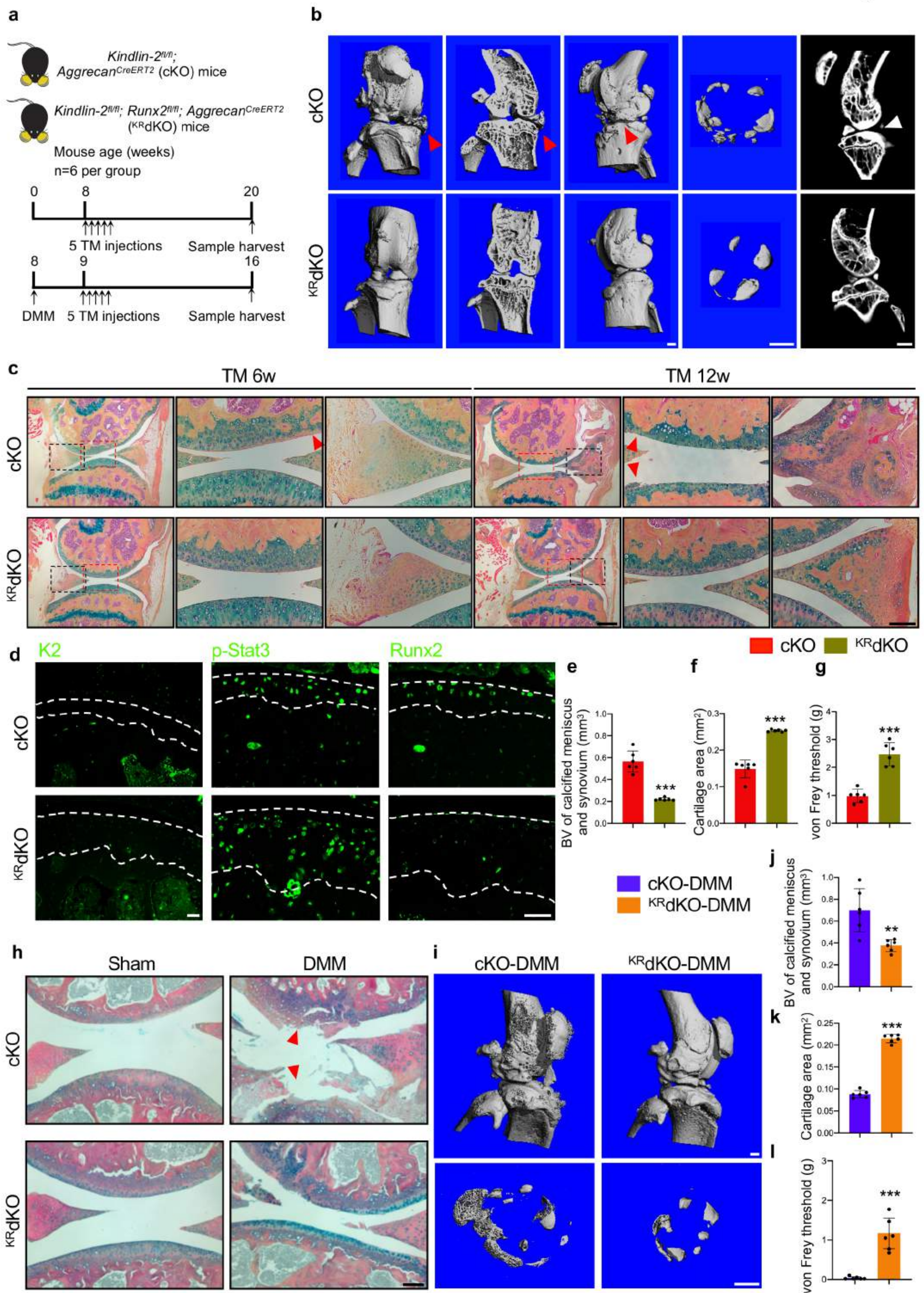

bioRxiv preprint doi: https://doi.org/10.1101/2021.08.11.456023; this version posted August 12, 2021. The copyright holder for this preprint (which was not certified by peer review) is the author/funder. All rights reserved. No reuse allowed without permission.

Figure 8